

EMEP /MSC-W
Date

Note 2/01
July 2001

DET NORSKE METEOROLOGISKE INSTITUTT
Norwegian Meteorological Institute

Research Report no. 57

The influence of scale on modelled ground level O₃ concentrations

Philippe Thunis

ISSN 0332-9879

Table of Contents

Preface and Acknowledgements

Executive Summary

1. Introduction
2. Objectives
3. Selection of the PIPAPO May 13th Episode
4. Grid and domain configurations
5. Meteorological modelling
6. Air Quality Modelling
7. Emission data
8. Analysis of the base-case
9. Impact of resolution on simulated chemical regimes
 - 9.1 Base case
 - 9.2 NO_x 40% reduction scenario
 - 9.3 VOC 40% reduction scenario
 - 9.4 VOC-NO_x chemical sensitivities
10. Impact of the emission inventories on air quality modelling
11. Impact of meteorological resolution on air quality modelling
12. Conclusions

References

Annex I: Transformation from EMEP to RACM species

Annex II: Conversion from MM5 data to the TAPOM grid

PREFACE AND ACKNOWLEDGEMENTS

This report results from the collaboration between the JRC (Joint Research Centre, Ispra, Italy) and the EMEP/MSC-W (Co-operative Programme for Monitoring and Evaluation of the Long Range Transmission of Air Pollutants in Europe, Meteorological Synthesizing Center West). This collaboration has been set up in view of contributing more efficiently to the objectives of the CAFE (Clean Air for Europe) programme launched by DG. ENV. This note may be seen as a first effort in trying to combine the regional modelling expertise of EMEP and the urban expertise of the JRC. It presents an analysis on the impact of spatial resolution on air quality modelling and related policies. In particular, this note addresses how the response of the model to different emission abatement strategies in urban centers depends on the spatial resolution of the model. The variability of the results due to the spatial resolution of emissions and meteorology is also investigated.

The Author wants to thank Asgeir Sortenberg, Erik Berge and Kees Cuvelier for their help in setting up and running the meteorological model MM5, Vigdis Vestreng and Ueli Joss for the preparation of emission data and Alain Clappier for his numerous advices with the TAPOM modelling system. Finally, the Author would like to deeply thank Leonor Tarrason for initiating this work and highlighting its objectives.

Executive Summary

One major concern at the European level is to design optimal emission reduction strategies in order to reduce in the most efficient way air pollution levels. This is true for many pollutants and in particular for ozone. Indeed, epidemiological studies have indicated a clear link between ozone concentration levels and health problems. Until now, European-wide policies have been elaborated based on regional air pollution modelling tools. Although these models have the advantage of covering most of Europe and therefore provide a European answer to the problem, they use a coarse resolution around cities that may result in non-optimal measures at the local level.

Spatial resolution in air pollution and meteorology modelling has always been a crucial issue. Ideally, simulations should use a resolution as fine as possible and a domain as large as possible to capture all processes. Unfortunately, this is prevented by CPU limitations. Therefore a compromise must be found between the resolution and the extent of the domain we want to simulate. The key issue consists thus in identifying the size of the relevant processes to determine the optimal scale and resolution. The goal of the present work is to check which resolution is necessary to simulate the relevant processes in air quality modelling around cities. One main policy related issue is:

Are regional scale based emission reductions sufficient to ensure the desired reduction of city air pollution levels or should additional local measures be taken?

To address this question, a local (meso) scale model that explicitly handles more city details is used with different spatial resolutions ranging from 50 to 4 km, i.e. characteristic of regional and urban scale models, respectively. Different emission reduction scenarios are then imposed. Unfortunately those local scale models are restricted to one city at a time and only for a few days simulations due to CPU demand limitations. In the present work, the city of Milan (Italy) has been selected for the particular episode occurring on May 13th 1998, as a large measurement dataset collected during the PIPAPO/LOOP field experiment is presently available for validation.

The influence of spatial resolution will be different whether we are concerned with peak or with (spatially, temporally or both) averaged values. For this reason, the impact of resolution on different indicators: peak concentration but also daily averaged AOT-40, 8h averaged AOT-60 and AOT-100 is investigated in this work.

Apart from the spatial resolution of the air quality model, the emission inventory and the spatial resolution of the meteorological dataset may also have an impact on the accuracy of the results. In this work, two different types of emission inventories: one regional at the EMEP scale and the other local at the fine scale are compared and simulations carried out with these two inventories are analysed. Meteorological datasets with different resolutions are also used and their impact on air pollution modelling investigated. The work is divided into three main sections dealing with these topics of which a brief summary is given here.

a) Impact of Air Quality Model resolution

For peak O₃ concentrations, differences of 20% were obtained between the 10 and 50 km resolution simulations whereas the 4 and 10 km simulation gave similar results. While peak concentrations were shown to be underestimated in coarse resolution simulations, 50 km spatially averaged concentrations were overestimated due to a larger dilution of the NO_x emissions in coarse grids that favours O₃ production. In summary, a 10 km resolution was shown to be sufficient to reproduce accurately both O₃ peak and AOT-40 and AOT-60 values. On the other hand, a 50 km resolution (i.e. regional scale models) produced accurate results for spatially averaged O₃ concentrations and for AOT-40.

The analysis of VOC and NO_x emission reduction in the Milan city indicated a tendency of coarser grids to underestimate the impact of a VOC emission reduction and to overestimate the impact of a NO_x emission reduction. This behaviour was shown to be more marked for the AOT-100 indicator than for the daily AOT-40 one.

b) Impact of the emission inventory

The significant differences in the NMVOC/NO_x ratio between the 50 and 3 km resolution emission inventory produced significant differences in air quality outputs. Indeed, Milan plume was only reproduced by the fine scale inventory and differences as large as 30 ppb in peak values were obtained. Note that both the NMVOC/NO_x ratio and the resolution are different in these two inventories. Further work will thus be necessary to estimate which of these two factors is more critical in explaining the large differences obtained in O₃ concentrations.

c) Impact of the resolution of meteorology

Finally, the comparison of air quality results obtained with different resolution meteorological datasets has shown a similar pattern for the pollution plume although differences in resolution ranged from 1.5 to 50 km. Even a very coarse resolution of 50 km was able to capture the main features of the atmospheric circulations in the Milan region. On the other hand, the variability of O₃ levels as simulated with the different meteorological resolution was shown to be large and at least as important as the variability associated with the resolution of the air quality model itself.

Although these conclusions are in theory valid only for the specific area of Milan and only for May 13th 1998, one can expect a similar behaviour in other conditions. It will be the purpose of further work to check how valid these conclusions are on the long term as well as for other cities in Europe .

1. Introduction

One major concern at the European level is to design optimal emission reduction strategies in order to reduce the most efficiently air pollution levels. This is true for many pollutants and in particular for ozone. Indeed, epidemiological studies have indicated a clear link between ozone concentration levels and health problems. Until now, policies have been elaborated based on regional air pollution modelling tools. Although these models have the advantage of covering most of Europe and therefore provide a European answer to the problem, they use a coarse resolution that may result in non-effective measures at the local level. This could be true especially where local scale circulations that are limited in their horizontal and vertical extent are present.

The key issue consists in identifying the size of the relevant processes to determine the optimal scale and resolution. The goal of the present work is to check which resolution is necessary to simulate the relevant processes in air quality modelling around cities (grid, emission, and meteorology resolution). More specifically, the questions we want to address are the following:

- Are European scale reduction policies useful at the local urban scale?
- Will simulated chemical regimes (i.e. NO_x versus VOC sensitive regimes) remain unchanged with different resolutions?

Obviously, the answer to those questions will vary according to the indicator we are interested in. The influence of resolution will indeed be different whether we are concerned with peak or with (spatially, temporally or both) averaged values. For this reason, the impact of resolution on different indicators (peak and various AOTs) is considered in this work.

In order to achieve these objectives, a mesoscale air quality model will be used with different resolutions. Unfortunately, those models are limited to the treatment of specific episodes. After selection of this episode, different emission scenarios will be imposed while varying the spatial resolution within the domain. Of course, being based on a single city and a single episode, this approach should not be seen as an attempt to provide a general answer to the question raised above but rather as a first step that should further be extended to other locations and episodes to gain spatial and temporal representativeness.

The first sections (1 to 6) describe the PIPAPO campaign and the modelling tools used in this work. The available emission inventories are described in Section 7. The May 13th base-case simulation is described in Section 8 whereas the impact of spatial resolution on simulated chemical regimes is investigated in Section 9. Finally Section 10 contains information on the impact of emission inventories and Section 11, information on the impact of the meteorological spatial resolution on simulated O₃ surface fields.

2. Objectives

Differences between regional and mesoscale air pollution model results can originate from various sources: emissions, meteorology, chemistry, ... The impact of the spatial resolution of each of these three factors is studied independently in this work. Indeed, in

order to better understand the impact of one factor, the others must be kept identical in all simulations. As an example, the same air pollution model and same emission inventory dataset are used to study the impact of the resolution of meteorology. With this in mind, here are in more details the objectives of this work:

- a. *Test the influence of the spatial resolution of the air quality model.* For this purpose, a series of simulation is carried out with different resolutions with the air quality TAPOM modelling system (see Section 6) on the same domain. The three spatial resolutions used in this work are of approximately 4, 10 and 50 km. Not only the influence of resolution is studied on mean concentrations but also on sensitivities with respect to emission reduction scenarios. Impact of these reductions is analysed on O₃ and on indicators such as AOT-40, 60, ...
- b. *Test the impact of the emission inventory.* Two different emission inventories are tested for the same region. The first is limited to the coarse resolution information (i.e. EMEP) whereas the second combines the available information from the fine scale emission inventory (resolution of 3 km) into the EMEP emission inventory.
- c. *Test the impact of the spatial resolution of the meteorology.* Three different types of grid resolutions, ranging from 1.5 to 50 km are used with the same meteorological model and their impact on air quality modelling is analysed.

3. Selection of the PIPAPO May 13th Episode

The city of Milan that is lying in the Po Valley, surrounded by the Alps, represents an interesting test case to address the problematic of resolution for two reasons. First, it is representative of cities that are influenced by locally driven meteorological conditions and as such susceptible to lead to divergent results between local and regional models. The second reason is the availability of a good measurement dataset gathered in 1998 within the frame of the LOOP-PIPAPO (Limitation of Oxidants Production – Pianura Padana Produzione di Ozono) field campaign.

The PIPAPO campaign aimed at evaluating both experimentally and numerically the production of O₃ and other pollutants between Milan and the Alps. The episode selected in this study is the one on May 13th. This episode was characterised by sunny conditions with the formation of a heat low over the Alps during the day. Thermally induced local circulations, i.e. slope winds directed towards the Alps were observed during the day and downslope winds were favoured during the night. During two of the Intensive Observation Periods (IOP), measurements were also carried out with airplanes in addition to the existing measuring network operated by local Authorities. The 13th May IOP was characterised by high pressure conditions over the whole Western Europe and a strong plume with concentrations reaching levels of 190 ppb about 35 km north of Milan was observed.

4. Grid and domain configurations

Emission data, meteorology data and models are not in general referring to identical grid systems. For what concerns the emissions, the EMEP emission inventory which has a 50x50 km resolution is based on a polar stereographic projection at 60 degrees north rotated by 32 degrees West. The finer scale emission inventories has a resolution of 3x3

km and is based on a Cartesian grid. The MM5 modelling system offers different choices of projections. It has been used with a polar stereographic 60 degrees projection but rotated differently, i.e. aligned on the central longitude of the coarser domain (8 deg. in our case). Three grids have been used (see Section below). The configuration of all those domains is shown in figure 1. The TAPOM model that is based on finite volume techniques may be used on any kind of grid systems. For ease, a Cartesian coordinate system has been chosen, relations between various projections and longitude/latitude values being given, it is then straightforward to transform them to a Cartesian coordinate system. Wind vectors are also transformed accordingly (see Annex II). The TAPOM modelling domain contains 17 levels along the vertical and 7, 35 or 84 grid points in X and Y according to the selected resolution

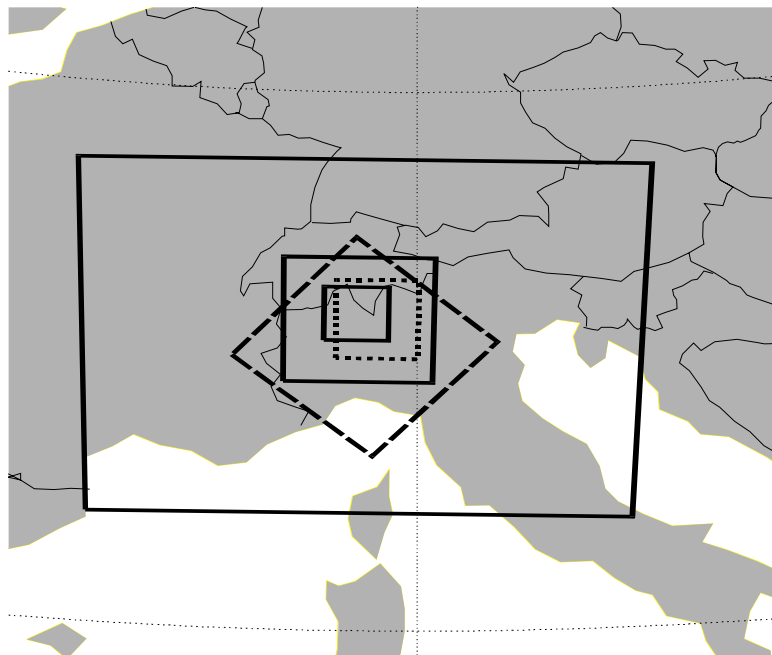


Figure 1: Representation of the grids used for meteorology, air pollution modelling and emission inventory. Solid rectangles show the meteorological MM5 grids with resolutions of 1.5, 4.5 and 13.5 km whereas the dashed lines delimitate the domain over which air pollution modelling (TAPOM) is operated. The dotted lines rectangle delimitates the area where fine scale emission information is available

5. Meteorological modelling

Meteorological data requested to drive the air pollution models are simulated by the mesoscale nonhydrostatic model MM5 (Grell et al. 1994). Three two-way interactive nested grids have been set up with the following characteristics: The outer grid has a resolution of 13.5 km and covers the Po valley including the whole alpine arc. Its total extension is 1070 x 820 km (79x61 grid points). The second domain that has a resolution of 4.5 km covers the Milan area and particularly its northern pre-Alps region. It covers an area of 290 x 290 km (64x64 grid points). The third and most inner domain is focused on the region where most measurements are available. Its resolution is 1.5 km and it covers an area of 120x120 km (82x82 grid points). The different grids are also shown in figure 1. For the three grids, the vertical extension of the domain is about 15 km and includes 31 levels. Boundary conditions are provided by 6 hourly ECMWF analyses. Simulations start

at 12 UTC on May 12th and last for 36 hours. Meteorological data from the three nests are interpolated to the TAPOM Cartesian grid coordinate system (see Annex II). For each of the TAPOM grid points, a value is obtained by interpolating the values from the four nearest neighbour locations (among the three MM5 nests). Necessary values are the wind speeds (u, v, w), potential and real temperature, pressure, density, humidity, Monin Obukhov length, friction velocity, land use, and topography. All simulations discussed in the following sections (except Section 11) are carried out according to this methodology and therefore use information from the same meteorological dataset.

6. Air quality modelling

The TAPOM air pollution model is an off-line evolution of the TVM-CHEM system that has been used in previous studies to simulate air pollution episodes in the area of Valencia, Spain (Thunis and Cuvelier, 2000) and Athens, Greece (Clappier et al., 2000). It is based on the chemical mechanism RACM (Stockwell et al., 1997) that includes 17 stable inorganics, four inorganic intermediates, 32 stable organics, and 24 organic intermediates, linked through 237 reactions. The numerical chemical solver is Gong and Cho (1993) that separates substances into "slow" and "fast" ones. The "fast" species are implicitly integrated with a Newton-Raphson integration scheme, whereas "slow" ones are explicitly integrated.

Pollutant transport is computed by a third order positive definite mass conservative scheme (PPM, Collela and Woodward 1984) corrected for multi dimensional applications (Clappier 1998) and extended for finite volume discretisation. This discretisation allows the use of any kind of structured grid based on 6-faces elements. Turbulence transport in the vertical direction is simulated using the K-theory with K values provided by the MM5 modelling system. Photolysis rate constants needed for the photochemical reactions are prepared by means of the Tropospheric Ultra-violet visible (TUV) sub module from the NCAR (Madronich et al. 1998). Dry deposition is calculated with the resistance analogy and is the inverse value of three resistances in series: the aerodynamic, the boundary layer and the surface resistances. Deposition velocities are calculated for each species and type of land surfaces. No wet deposition is currently implemented.

7. Emission data

Emission data are available from two different sources:

- a. The finer scale emission inventory that covers approximately 150 x 150 km has been put together by the ASL Lecco-Regione Lombardia and Meteotest/BUWAL in the frame of the EUROTRAC-LOOP PIPAPO project. It provides a 3x3 km inventory with an hourly resolution. NMVOC species are split into 32 classes. Those 32 classes are lumped into the TAPOM-RACM speciation according to Middleton et al. (1990). As mentioned above, this inventory is based on a Cartesian grid.
- b. The EMEP inventory covers all Europe with a 50x50 km resolution. Yearly gridded data are available for SO_x, NO_x, NMVOC, and CO at a SNAP 1 level (Vestreng and Storen 2000). The sector repartition of the emissions is used to split NMVOC into the EMEP species. Those EMEP emissions are converted to the RACM speciation based on the National Acid Precipitation Assessment Program (NAPAP) emission inventory values. Examples are given in Annex I. EMEP emissions are given in Tons/year/EMEP_cell that are converted to

hourly values assuming a uniform repartition among the days as well as during the course of the day.

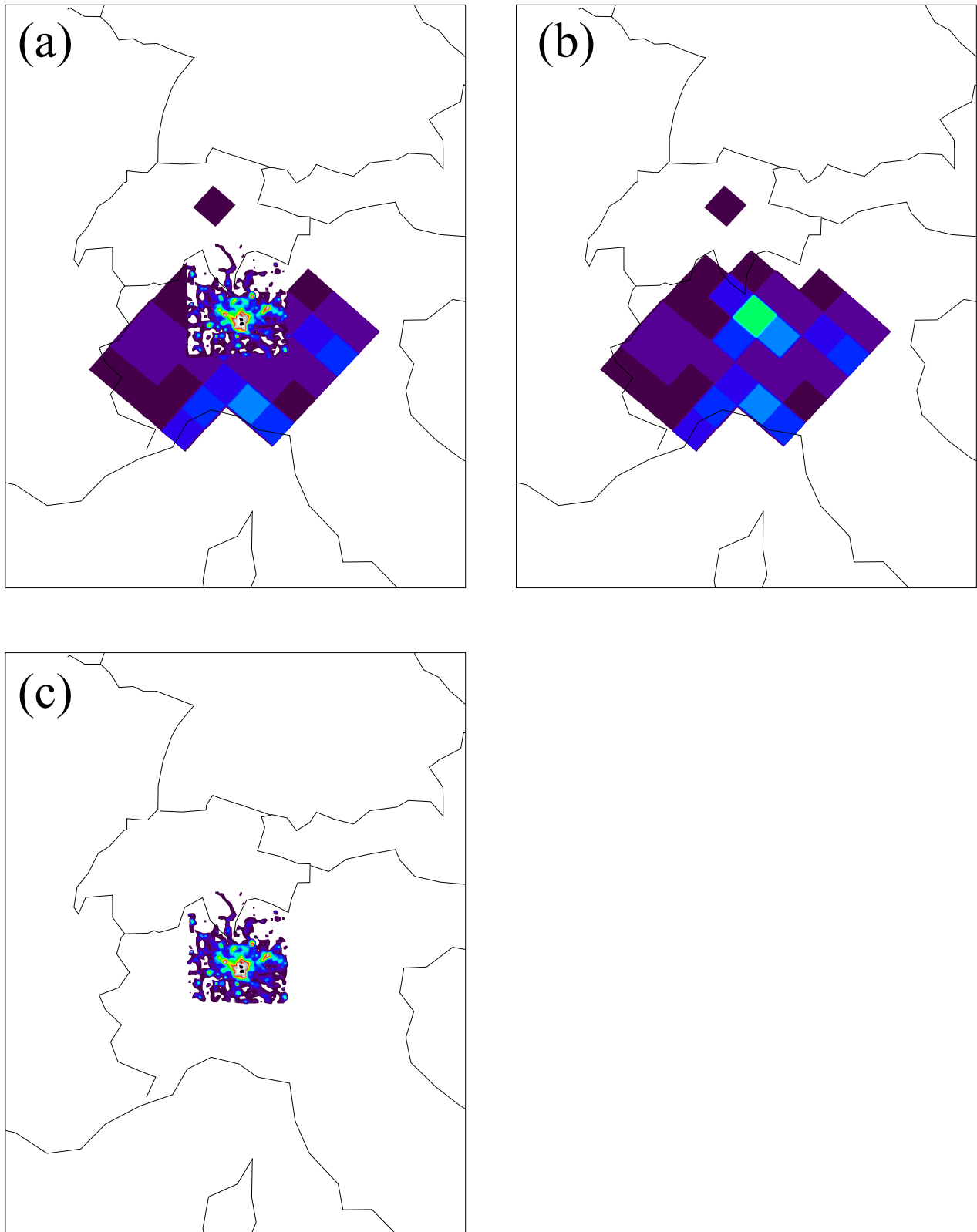


Figure 2: Representation of the different emission inventories in the EMEP projection. (a) Total emission inventory, i.e. sum of the fine and EMEP scale inventories, (b) EMEP inventory and (c) fine scale inventory.

In this work, the fine scale emission inventory has been interpolated into the EMEP type of projection. Practically, each EMEP grid is divided into a certain number of cells for which combined emissions are calculated. Those cells are the ones that will finally be used in our TAPOM calculations. To combine emissions, each of those TAPOM cells is at its turn subdivided by 100 and for each of these 100 cells, a check is made to see whether or not fine scale emissions are present at that specific location. A covering percentage of the fine scale emission is then obtained for each TAPOM cell, the rest of the emissions being given by the EMEP emissions. Figure 2 shows how the two types of emission inventories (plotted in the EMEP projection grid) are shaping up as well as the combined emission inventory. The EMEP based inventory covers the whole area in which two main area emission sources can be identified: Milan and Genova. Fine scale emissions only cover the Milan area. Local emission peak values in the fine scale inventory are of course much higher than EMEP ones as those represent a uniform distribution of the 50x50 km resolution base EMEP inventory.

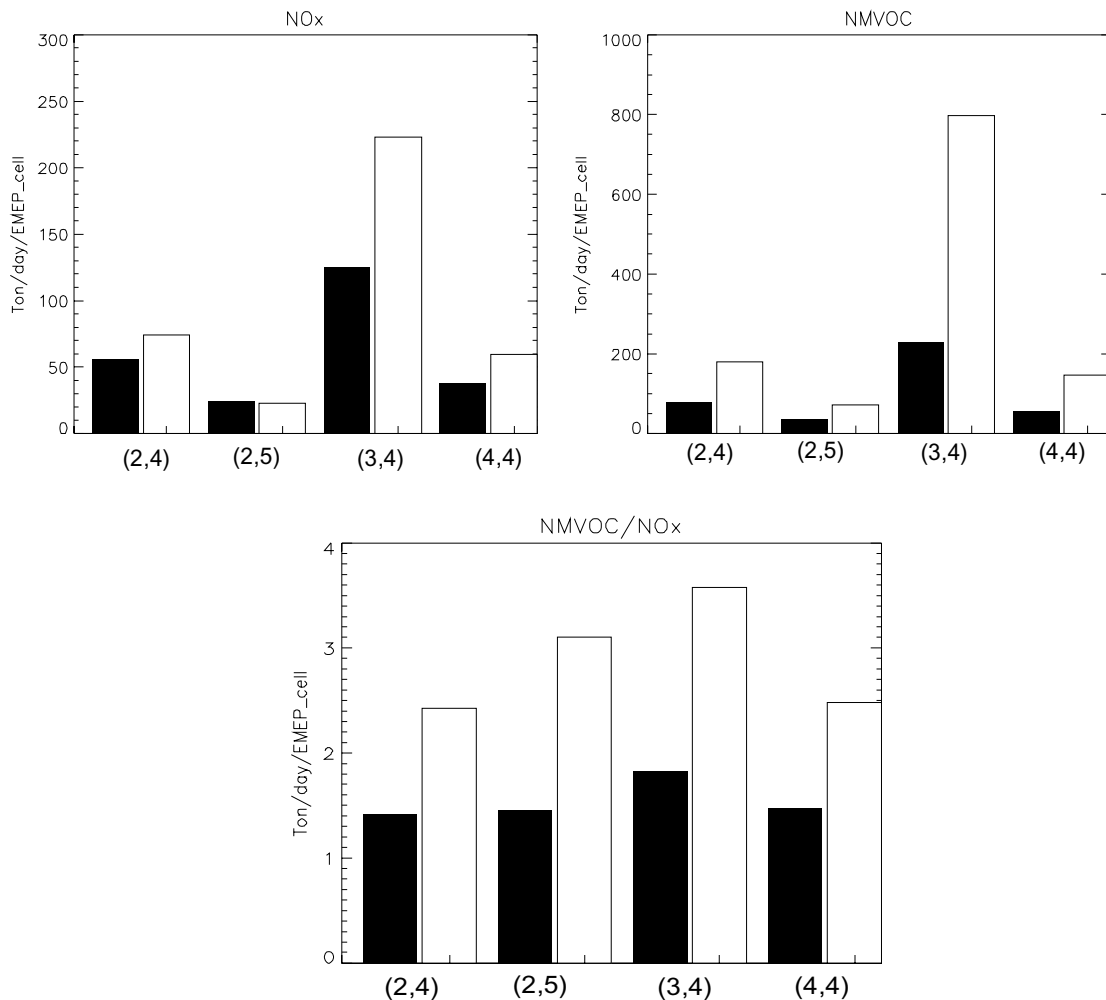


Figure 3: Comparison of EMEP (Black) vs fine scale (White) emission cell totals for NMVOC, NOx, and the ratio NMVOC/NOx for four different EMEP cells. Cell (3,4) includes Milan city (see cell reference in Figure 4).

A comparison between the fine and EMEP scale emission inventory for NMVOC and NOx is shown in Figure 3, for 4 different EMEP 50x50 km cells in the domain (cell [3,4]

includes Milan City). For this comparison, fine scale emissions within each EMEP cell have been summed and compared with EMEP emissions. While totals for CO (not shown) are close in the two emission inventories, the fine scale inventory shows much larger values for SO_x (not shown) and NO_x and especially for NMVOC. For this latter one, a factor of two difference is observed for certain cells. The ratio NMVOC/NO_x is also higher in the fine scale than in the EMEP emission inventory. Further work would here be needed to better understand where these differences are arising. A first step (in progress) is to screen the inventories by activity sector to identify the main discrepancies.

8. Analysis of the base-case

The synoptic conditions on May 13th are characterised by a long lasting high-pressure system over the Alps. Observations show the formation of downslope flows during the night in the Alps and of upslope flows during the day. Winds are generally weak near the surface and especially nearby Milan City. MM5 results reproduce these circulations although they are over-estimated during the night and under-estimated during the day. During the night, MM5 predicts the formation of mountain waves generated by the high wind speeds in altitude over the Alps that influence surface conditions. Nighttime wind speeds are relatively high even within the Po valley. During the day, a general upslope flow is generated within the Po Valley but is generally weaker than showed by observations.

For what concerns photochemistry, two areas may be distinguished with respect to emissions, the Genova and Milan areas. At Milan, primary pollutant emissions are pushed towards the SW during the night whereas they move N-NE during the day. Two pollution clouds are formed, a first one resulting from the transformation of the evening and nighttime primary pollutant emissions, the second peak being generated from the primary pollutants emitted in the morning. The second of these peaks reach the pre-Alps region in the late afternoon. The simulated Milan plume reaches maximum concentrations of the order of 170 ppb in the late evening, which are close to observations (around 190 ppb). However, the plume trajectory as shown by the observations is not exactly reproduced by the model, the simulated plume passing too much East. This discrepancy between observed and measured concentrations is probably due to the problems encountered in simulating the wind field regimes in this area. Note that the presence of the Alps leads to serious problems, one of them being the smoothing of the topography implicitly accounted for by the resolution. The simulated roughness generated by the Alps tends to be underestimated in the simulation. This could explain the overestimation of the wind velocities at night. On the other hand, during the day, temperature in the pre-Alps stations all exhibit higher temperatures from those simulated which could explain at least partly the underestimation of the up-slope winds over the Po valley during daytime.

9. Impact of resolution on simulated chemical regimes

9.1 Base case

As mentioned above, three different resolutions have been used to simulate this episode. The three resolutions correspond to EMEP grid cells being divided in 1 (R1), 5 (R5) and 12 (R12), respectively. These dividing factors lead to resolutions of approximately 50, 10 and 4 kilometres. Figure 5 shows a comparison of the O₃ simulated fields at 17:00 LST with the three different resolutions. At this particular time, O₃ concentrations are close to their afternoon maximum. Apart from the lack of detail that can be expected, an

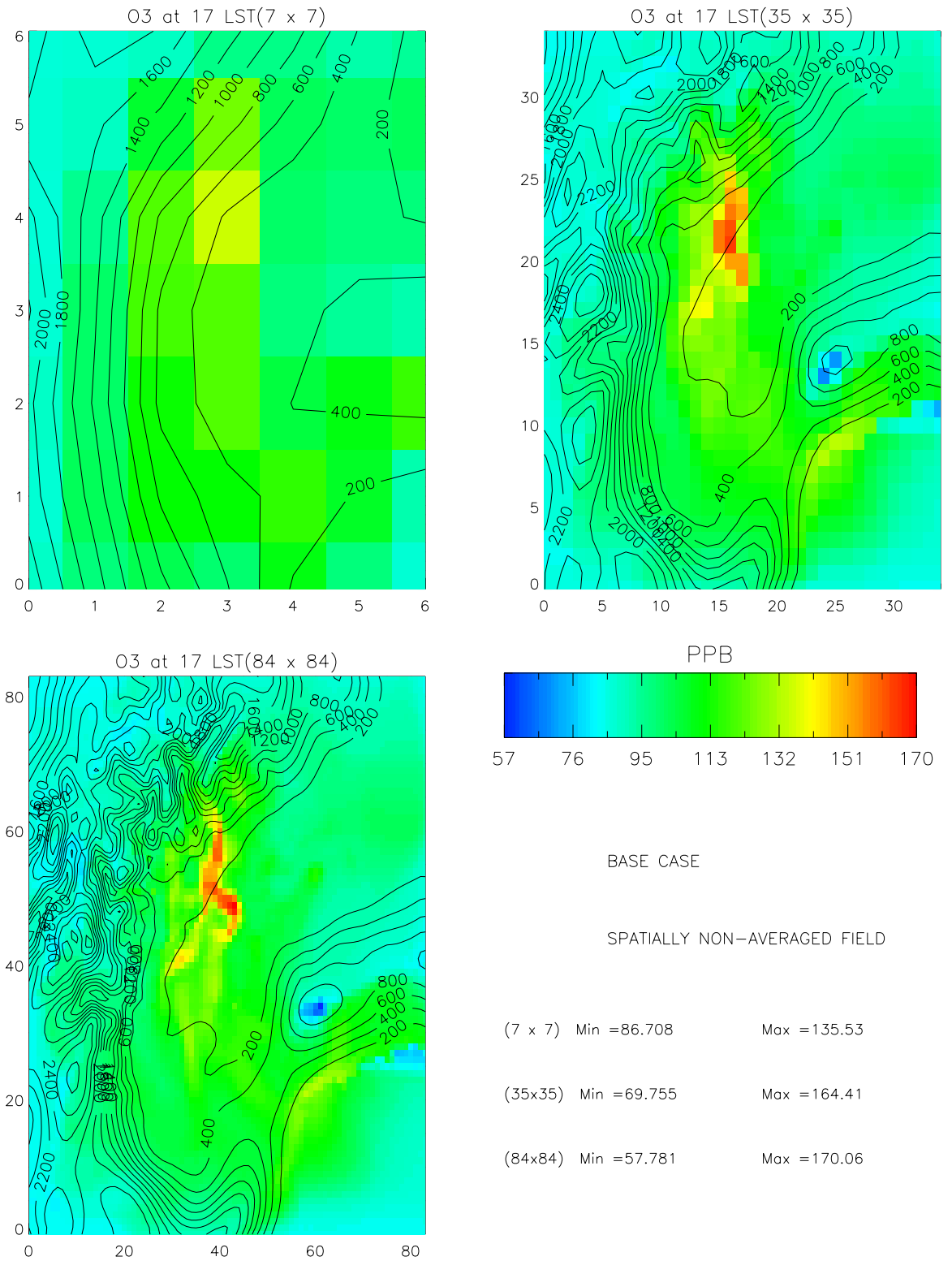


Figure 5: Comparison of the O3 field at 17:00 LST for the three different resolutions. Results are shown for R1 (top left), R5 (top right) and R12 (bottom left).

underestimation of the ozone peak when the resolution is coarser is observed. Indeed, while R12 indicates a maximum of 170 ppb, R5 and R1 show maximum values of 164 and 135 ppb, respectively. This leads to an underestimation of 20 and 4 % for R1 and R5, respectively. It can be noted that the 10 km (R5) and 4 km (R12) simulations produce very similar results indicating that a 10 km resolutions would be sufficient to capture peak ozone concentrations. The position of the plume, despite differences in resolution is quite similar in all three simulations. In the morning (10:00 LST, not shown), the simulated O3 values for R1, R5 and R12 are given by: 92, 107 and 125 ppb, respectively. The coarser resolution simulation R1 thus underestimates by 25 and 20% the maximum O3 values at 10:00 and 17:00 LST. Those figures are on the order of 14 and 4% for R5. A temporal evolution of the maximum O3 concentrations obtained with the 3 different resolutions is shown in figure 4 (a).

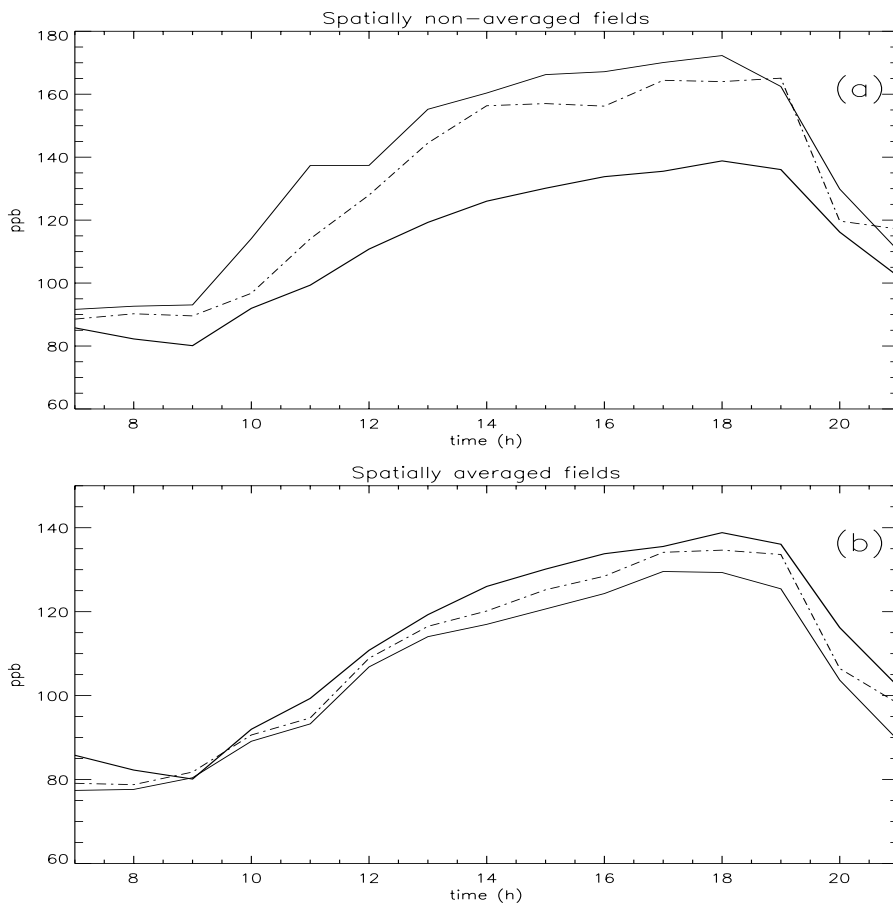


Figure 4: Time evolution of the simulated O3 maximum for R1 (thick line), R5 (dashed line) and R12 (solid line) for (a) non-spatially and (b) spatially averaged concentrations

When averaged over the same spatial resolution, i.e. the R1 grid, results are almost similar but the coarser simulation now tends to slightly overestimate the correct value (supposed to be the finer resolution one). This overestimation is due to the fact that precursors (especially NO_x) are more diluted into the large cells of the coarse grid. Consequently, the ratio NO_x/VOC is more favourable to ozone formation. A time evolution of the spatially averaged maximum values is shown in figure 4 (b) and it shows that this overestimation of the coarse resolution model is present during the whole day.

National Emission Ceiling Protocols, based on the analysis of the adverse effects from ozone, are based on different types of indicators among which AOT 40 and 60 are commonly used for vegetation and health protection, respectively. Other indicators for information or alert to the population are also used. All those indicators being based on different time averages, it was decided in this work to test the impact of resolution on the following three different indicators: AOT 40 (daily average), AOT 60 (8h average) and AOT 100.

- *AOT 40 (daily average)*: If no spatial average is made (Fig. 6), the AOT 40 peak values obtained with R12 and R5 are almost identical (~ 0.4% difference) whereas R1 underestimates the peak by 12% (see Table 1). As for O₃ concentrations, however, the position of the AOT 40 maximum is similar with all three resolutions and is located north of Milan in the Lake region. If those daily-averaged results are also averaged in space (i.e. aggregated to the EMEP resolution) similar values are now obtained for the three resolutions (difference ~ 3%). These results indicate that a resolution of 10 km (R5) and even 50 km (R1) would be sufficient for dealing with AOT-40 related policies. One should remember, however, that this conclusion is valid only for Milan and for the specific episode considered in this study.
- *AOT 60 (8h average from 12:00 to 19:00 LST)*: If no spatial average is made (Fig. 7), the AOT 60 peak values are underestimated by 6% by R5 and by 26% by R1 (see Table 1). The position of the maximums is now also located in the Lake region but is also extending much more in direction of Milan. When spatially averaged, 8h-AOT 60 values are now overestimated both by R1 (17%) and R5 (7%). Here also, differences between a 10km and a 4km resolution are not very significant.
- *AOT 100 (at 17:00 LST)*: If no spatial average is made (not shown), differences become now very significant. Peak values are underestimated by almost 50% for R1 and 8% for R5 whereas when spatially averaged, overestimation is now of the order of 20% and 15% for R1 and R5 respectively.

In summary, a clear *underestimation* of the ozone peaks is seen when resolution becomes coarser. This conclusion remains valid for other types of indicators such AOT40, 60 and 100 for different length of time averaging. On the other hand, when results are spatially averaged on the same coarser grid, a systematic *overestimation* shows up. It is not significant for peak O₃ values and day-AOT40 but becomes significant for 8h-AOT 60 when the coarser resolution (R1) is considered and for AOT 100 for both R1 and R5. These results indicate that for this episode, a 10 km resolution (R5) seems sufficient to capture both O₃ peaks and AOT-40 and AOT-60 values correctly whereas the 50 km resolution (R1) reproduces accurately O₃ spatially averaged concentrations and AOT-40.

In the following sections, different emission scenarios are now discussed. The objective is to check whether or not local emission reductions would have a similar effect in a regional and in a mesoscale model. This point is investigated by performing emission reduction

only for the Milan city that mainly occupies one EMEP grid cell. For this particular cell, 40 % VOC and NOx reductions are independently considered. Note that this 40 % reduction of NOx and VOC, respectively represent a reduction of 5 and 11% of the domain total NOx and VOC emissions

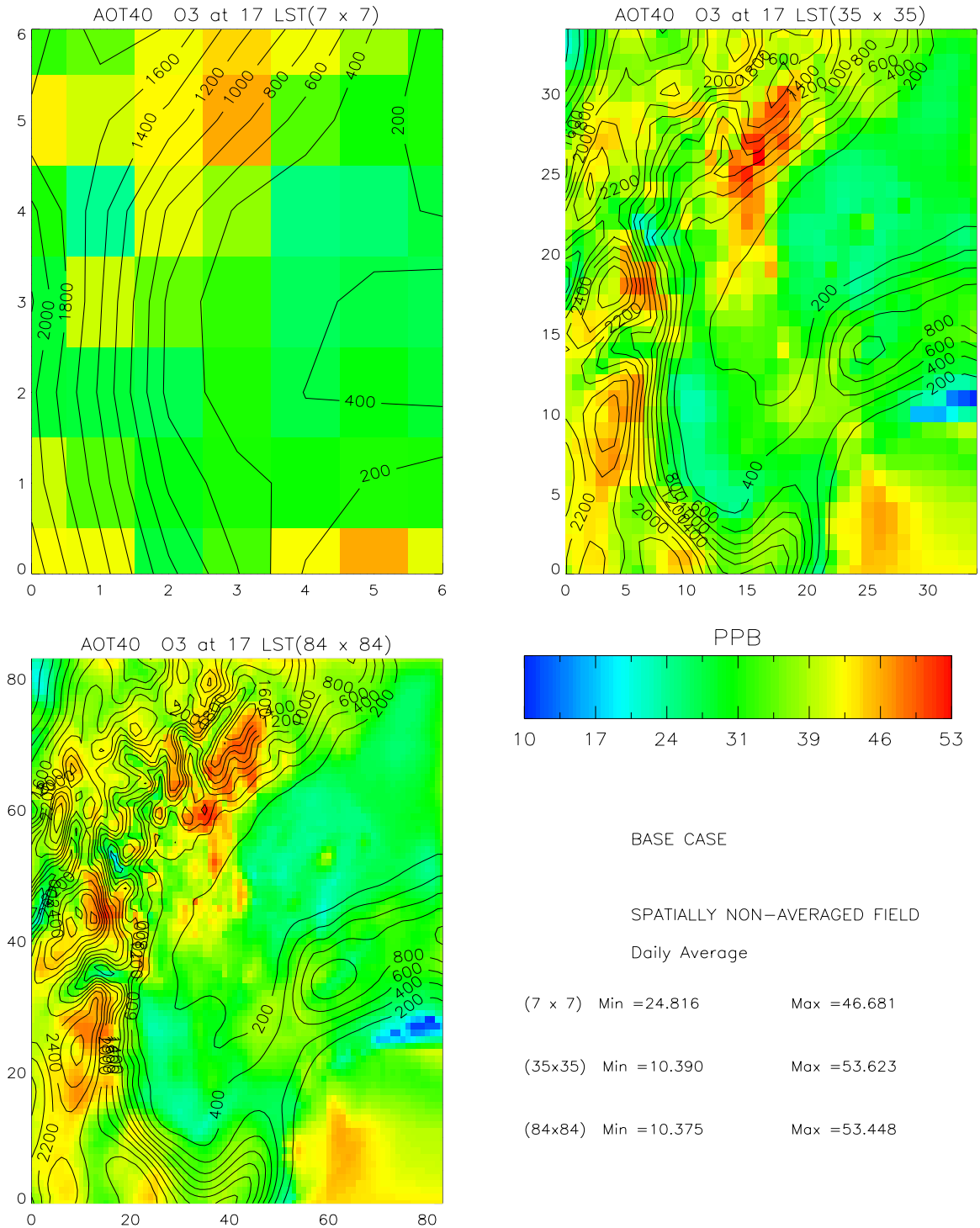


Figure 6: Comparison of the daily AOT 40 values for the three different resolutions. Results are shown for R1 (top left), R5 (top right) and R12 (bottom left).

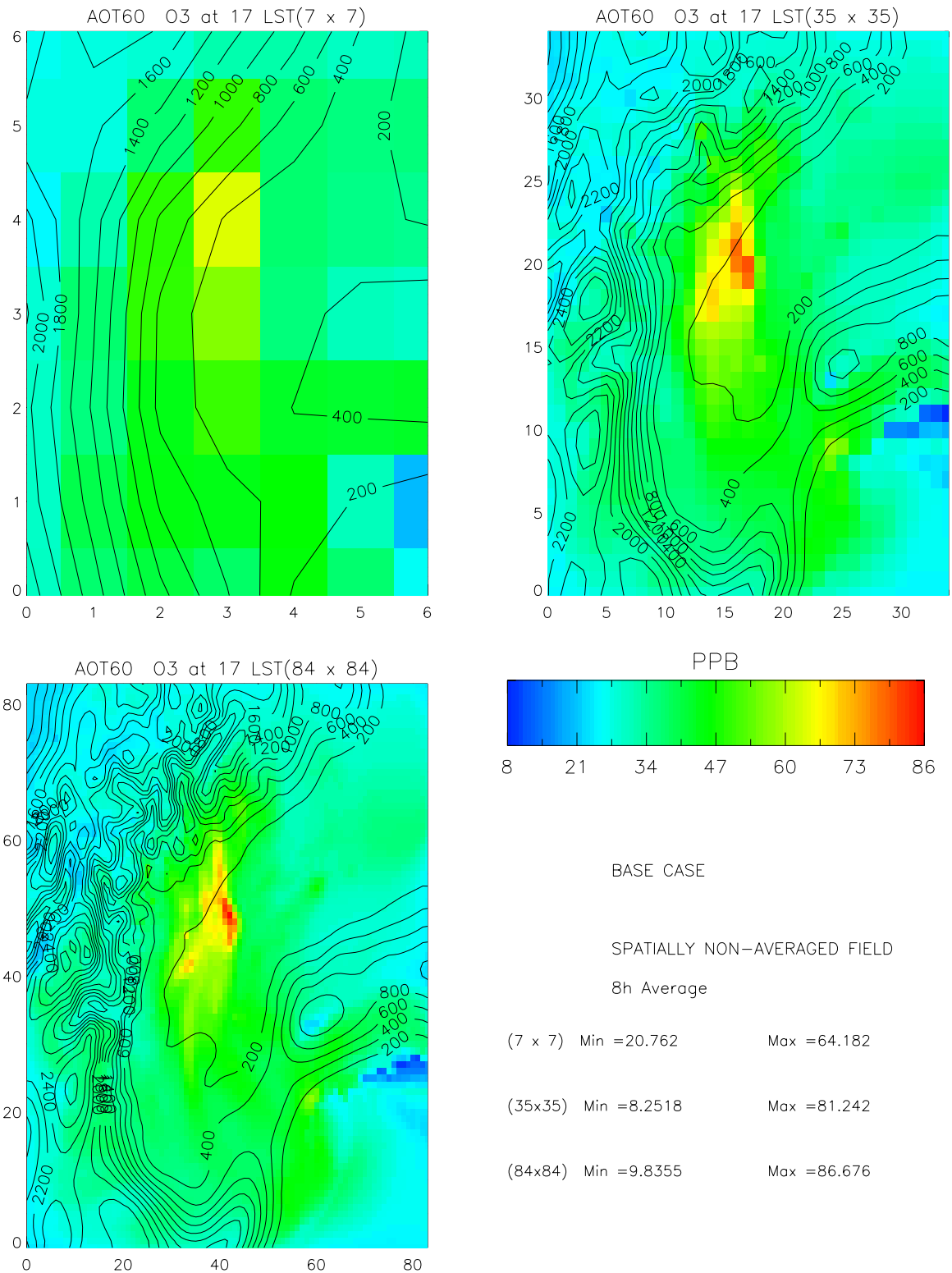


Figure 7: Comparison of the 8h AOT 60 values for the three different resolutions. Results are shown for R1 (top left), R5 (top right) and R12 (bottom left).

9.2 *NO_x 40 % reduction scenario:*

At 10:00 LST, O₃ peak values are larger than in the base case and reach: 97, 122 and 139 ppb for R1, R5 and R12, respectively which represents increases of 5 ppb (5%), 15 ppb (14%) and 14 ppb (11%). These differences are representative of the peak values but can be locally much higher: 17, 24 and 37 ppb for R1, R5 and R12 respectively.

At 17:00 LST, peak values are now 125, 146 and 150 ppb for R1, R5 and R12 showing now a clear decrease in all three simulations as compared to the values obtained in the base case. The obtained reductions on peak concentrations are on the order of 10 ppb (8%), 18 ppb (12%) and 20 ppb (13%) for R1, R5 and R12 respectively. As was observed previously the coarse resolution simulation tends to underestimate O₃ concentrations but it also underestimates the impact (difference) of an emission reduction. The temporal evolution of the differences and averaged differences is shown in figure 8.

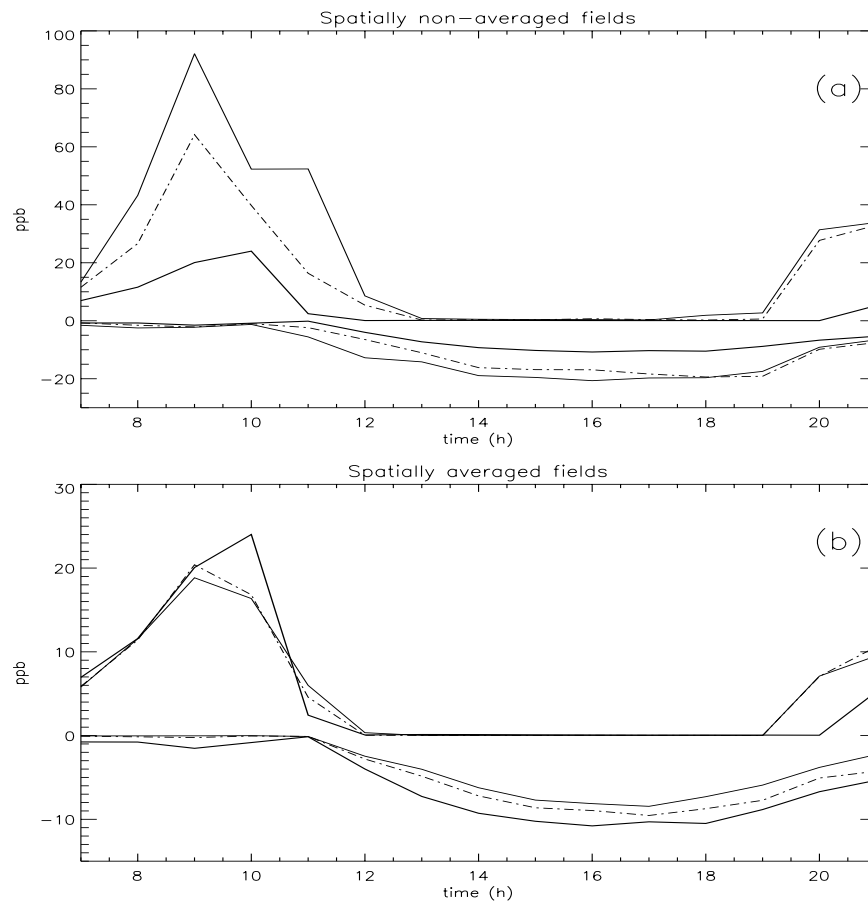


Figure 8: 40% NO_x Scenario: Time evolution of the (NO_x –Base Case) differences for R1 (thick line), R5 (dashed line) and R12 (solid line) on spatially non-averaged (a) and averaged (b) O₃ peak values. The two set of curves correspond to the maximum and minimum differences

If we now consider the spatially averaged values for this scenario, concentrations are then overestimated in the coarser simulations. This conclusion is also valid for the differences which are equal to 24, 17 and 16 ppb, for R1, R5 and R12 respectively at 10:00 LST. The same behaviour is observed at 17:00 LST although spatially averaged impacts are much closer.

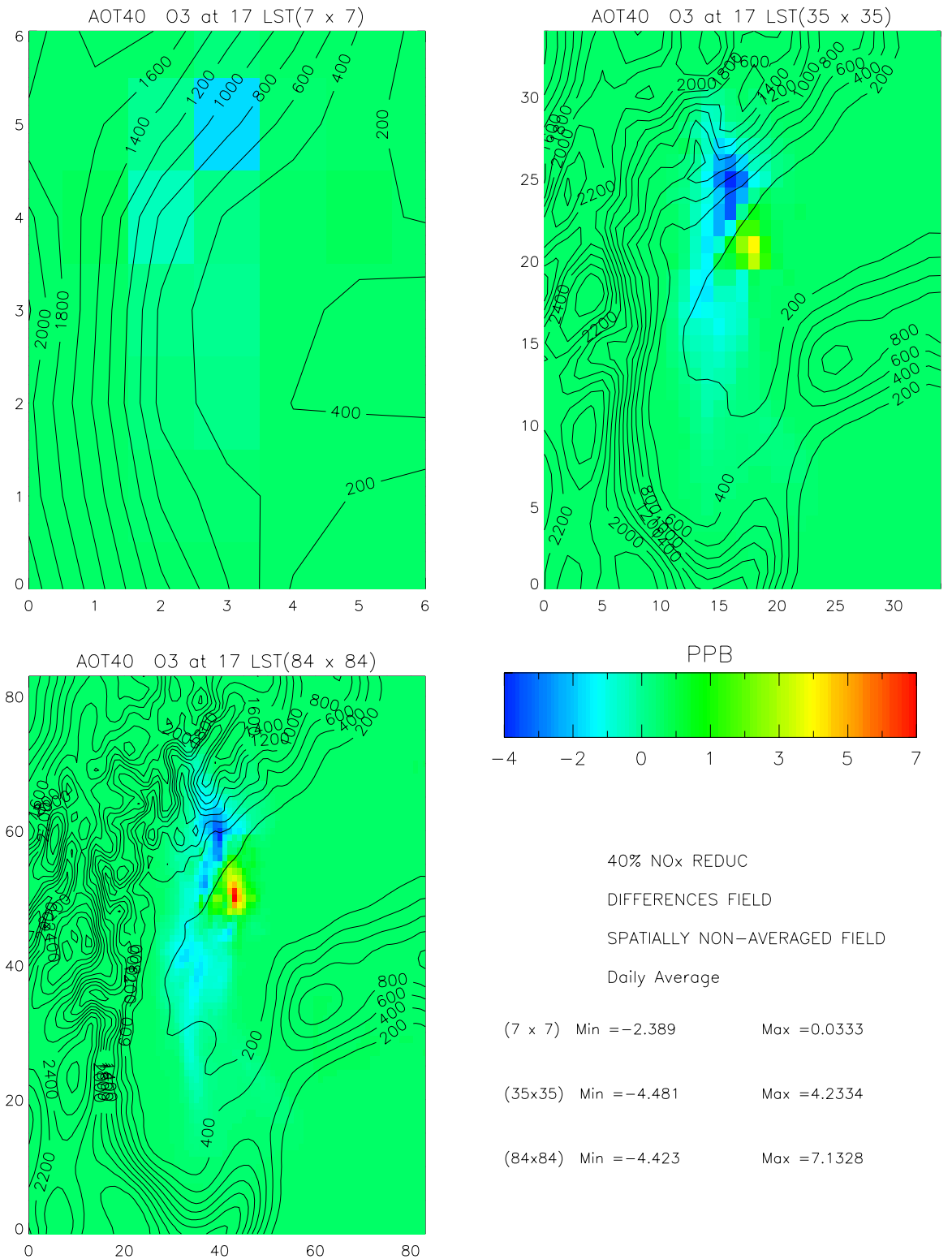


Figure 9: Comparison of (NO_x -Base) differences on daily AOT-40 values for three different resolutions

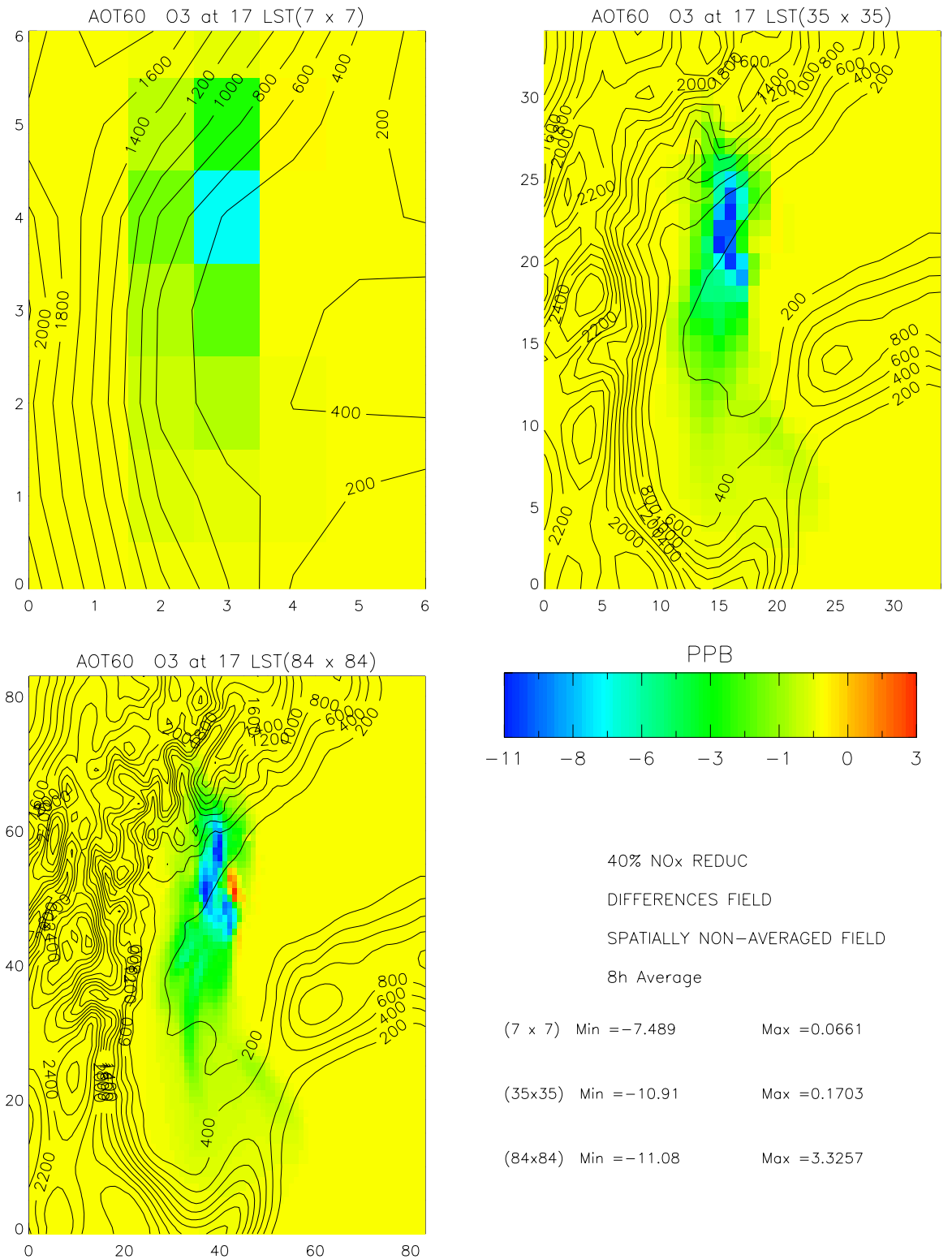


Figure 10: Comparison of (NO_x -Base) differences on 8h AOT-60 values for three different resolutions.

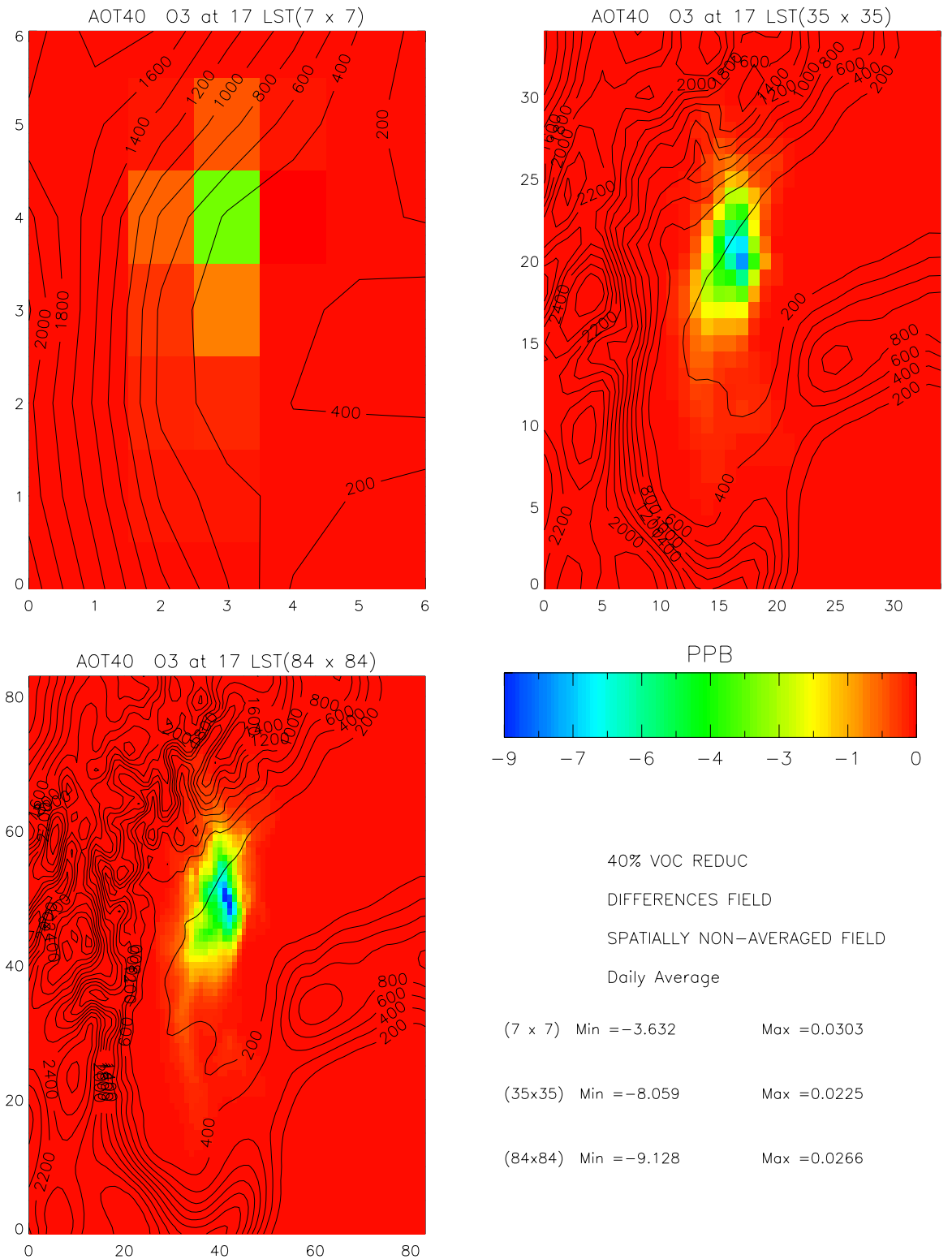


Figure 12: Comparison of (VOC -Base) differences on daily AOT-40 values for three different resolutions

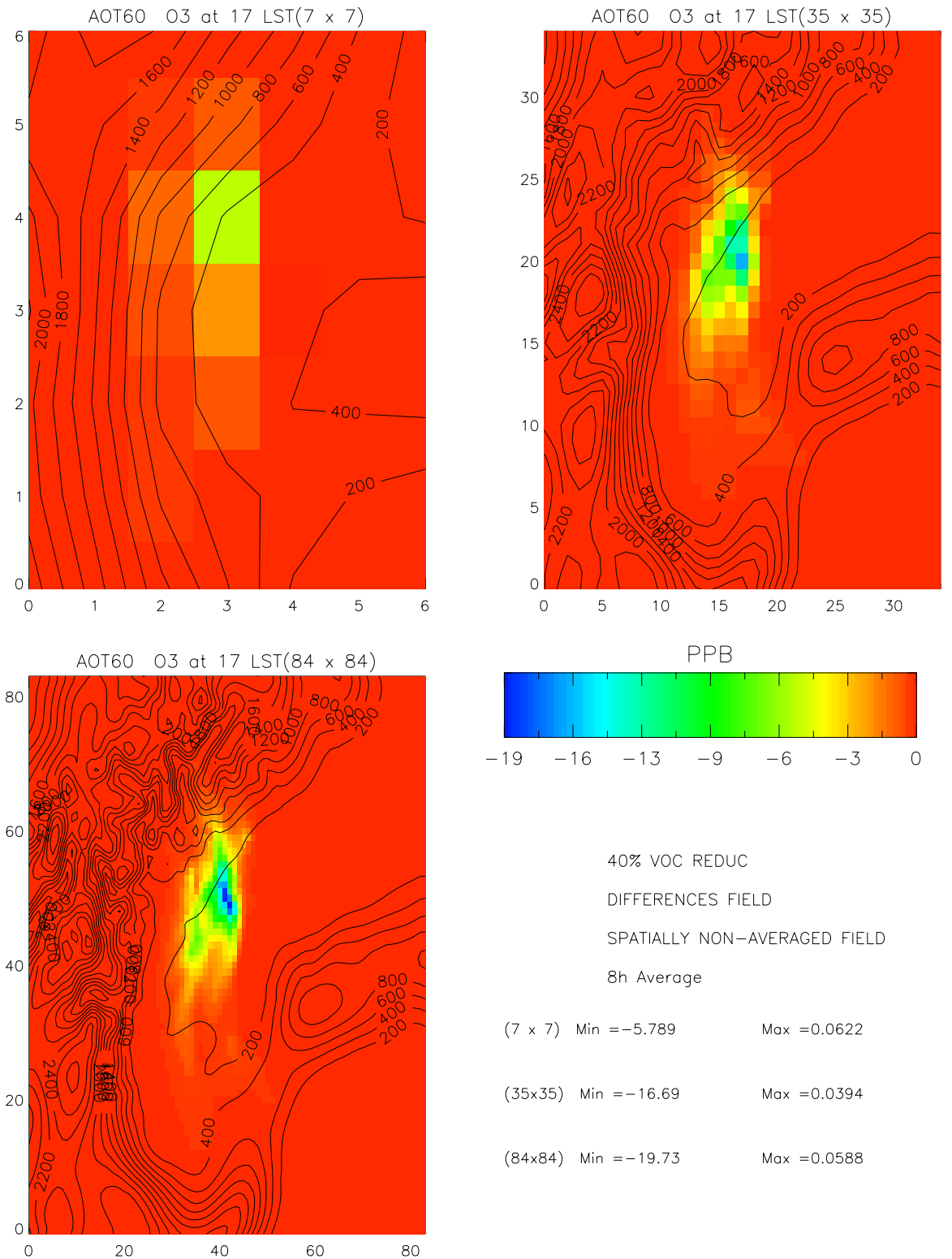


Figure 13: Comparison of (VOC -Base) differences on 8h AOT-60 values for three different resolutions

Figures 9 and 10 show the impact of resolution on NO_x regimes for two indicators mentioned in the previous section: 24h-AOT40 and 8h-AOT60. The *daily AOT-40 map* shows both a NO_x negative and positive sensitivity areas in R12 and R5 but only a negative sensitivity area for R1. Increases in O₃ due to NO_x emission reductions are mainly observed in and around Milan city whereas decreases are observed further away from the city (with a maximum in the Lake region). The peak intensity of the positive area is underestimated by 40% by R5 whereas R1 does not see it at all. For the negative area, peaks are similar for R5 and R12 but underestimated by 45% for R1. In the *8h AOT-60 map*, positive sensitivity areas disappear and peak minimum values are much closer. Underestimation is now of 10% for R1 whereas similar reductions are obtained for R5 and R12. The same conclusions are valid for the *AOT-100 map* (not shown).

The comparison of coarse and fine scale spatially averaged results (not shown) shows that the coarse resolution ones tend to underestimate both the maximum values and the differences. These two underestimations combine to lead to O₃ coarse peak concentrations that are close to fine scale spatially averaged concentrations for the 40% NO_x emission reduction scenario. Table 1 summarises the O₃ values for different resolutions and scenarios and quantitatively estimates the difference between R1, R5 and R12.

9.3 VOC 40 % emission reduction scenario:

At 10:00 LST, O₃ peak values are similar for R1 and R5 to those of the base case but are lower for R12 with a value of 96 ppb which represents a decrease of about 15% (18 ppb).

At 17:00 LST, peak values are now 132, 151 and 158 ppb for R1, R5 and R12 showing now a clear decrease in all three simulations as compared to the values obtained in the base case. The obtained reductions on peak concentrations are on the order of 3 ppb (3%), 13 ppb (8%) and 12 ppb (7%) for R1, R5 and R12 respectively. As was observed previously the coarse resolution simulation tends to underestimate O₃ concentrations but it also underestimates the impact (difference) of an emission reduction. The temporal evolution of the differences and averaged differences is shown in figure 11. Note that a NO_x emission control tends to be more efficient than a VOC control for what concerns peak O₃ values. It must also be noted that the differences between different resolution simulations tend to be larger in the early morning than in the afternoon (as was the case for the NO_x scenario (Fig. 8) and for O₃ concentrations (Fig. 4)). In the morning, peak ozone concentrations are observed closer to the city where the chemical regime is NO_x dominated. Under those conditions, a 10 km resolution seems insufficient but one should remember that peak O₃ concentrations are then not as large as those observed in the afternoon.

If we now consider the spatially averaged values for this scenario, concentrations are again slightly overestimated in the coarser simulations. This conclusion is also valid for the differences which are equal to -26, -15 and -13 ppb, for R1, R5 and R12 respectively at 10:00 LST. At 17:00 LST, the same behaviour is observed for the spatially averaged concentrations but averaged differences are now lower in the R1 than in R5 and R12.

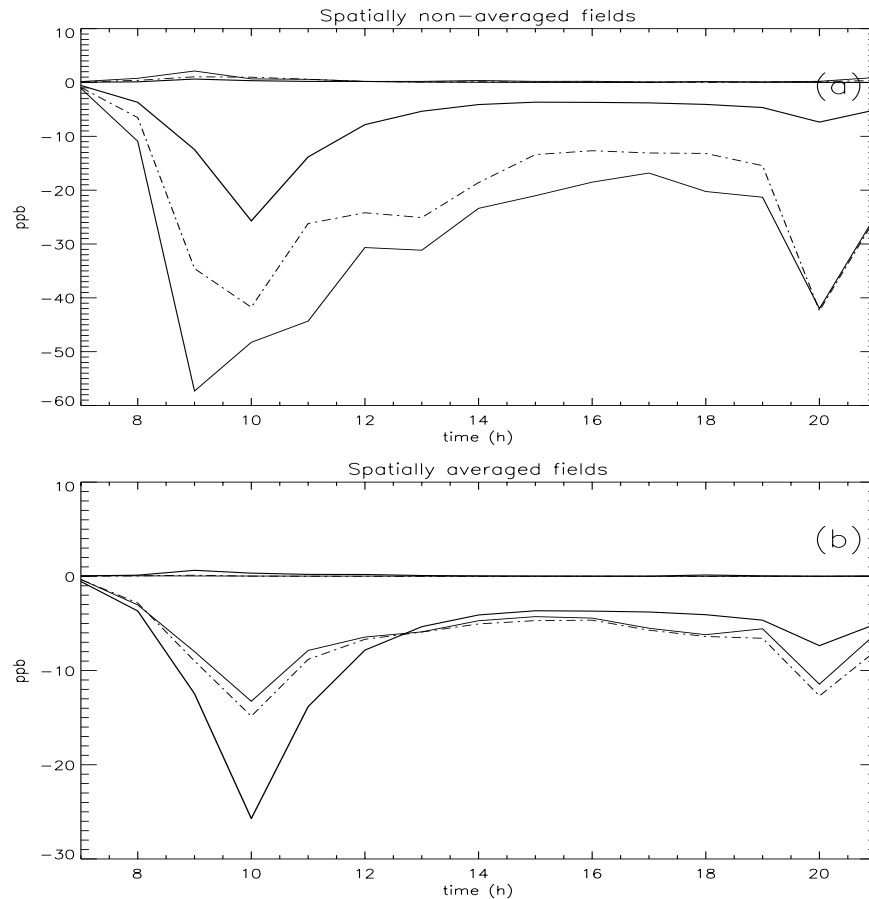


Figure 11: 40% VOC scenario: Time evolution of the difference in O₃ (VOC - Base Case) for R1 (thick line), R5 (dashed line) and R12 (solid line) for spatially non-averaged (a) and averaged (b) values. The two sets of curves correspond to the maximum and minimum differences.

Figures 12 and 13 show the impact of resolution on VOC regimes for 24h-AOT40 and 8h-AOT60. For both, only a negative sensitivity region is simulated (i.e. a reduction of VOC emissions never lead to increase of O₃). The *daily AOT-40 map* shows that R1 and R5 underestimate the peak by 60 and 12%, respectively. These underestimations are of the order of 37 and 8% for the 8h AOT-60 and of 17 and 5% for the AOT-100

The comparison of coarse and fine scale simulations show that spatially averaged concentrations (not shown) are larger in the coarse than in the fine resolution. While spatially averaged differences exhibit the same behaviour during the morning hours, it is reversed in the afternoon. At that time, differences in the O₃ spatially averaged concentrations between the three different resolutions are larger than they were in the NO_x case. Table 1 summarises the O₃ values for different resolutions and scenarios and quantitatively estimates the difference between R1, R5 and R12.

9.4 *VOC-NOX chemical sensitivities*

The efficiency of a VOC versus a NOx emission reduction is estimated by calculating the difference between the following simulations: (VOC – Base Case) – (NOx – Base Case) = VOC – NOx. Whenever this difference is positive, the chemical regime will be NOx sensitive in that a reduction of NOx is more efficient than a similar VOC reduction in reducing O3 concentrations. If negative, the chemical regime will be VOC sensitive. As seen from figure 14, where chemical regimes are shown for O3 at 17:00 LST, a VOC sensitive regime is simulated in and nearby Milan city whereas a NOx sensitive regime is produced further north (and in a less significant way south) of Milan. The maximum O3 concentrations are simulated along the separation line between those two regimes.

Figure 15 show how chemical regimes are simulated for daily AOT-40 with the three different resolutions. All resolutions give NOx sensitive regimes of similar intensities although slightly underestimated in R1. The intensity of the VOC sensitive regime, however, is largely underestimated in R1 (> 100%). The same behaviour is observed for both the 8h AOT-60 and the AOT-100 indicators (not shown) but with a larger decrease of the VOC-sensitive area and a larger underestimation of the NOx regime. In summary, both NOx and VOC regimes are underestimated by coarser resolutions but in a stronger way for the VOC ones.

When results are spatially averaged (Figure 16), the tendency of a coarser resolution is to underestimate the intensity of the VOC sensitive regime and to overestimate the intensity of the NOx regime for the daily AOT-40. The same conclusion holds for O3, 8h AOT-60 and AOT-100. This behaviour is in agreement with the results discussed in the NOx and VOC emission reductions sections where it was shown that spatially averaged differences were underestimated by a coarser resolution in the VOC scenario and overestimated in the NOx scenario (see figures 8 and 11). The effect of the decrease of resolution is to dilute the precursors in a way that brings the polluted air mass in a concentration range close to the one that characterises the transition between the VOC and NOx sensitive regimes. Consequently, the extension of the VOC sensitive regime is considerably reduced and O3 production is more efficient. Moreover, due to the fact that the O3 chemical production is closer to an optimum at lower resolutions, the impact of a NOx emission reduction is larger than for finer resolutions.

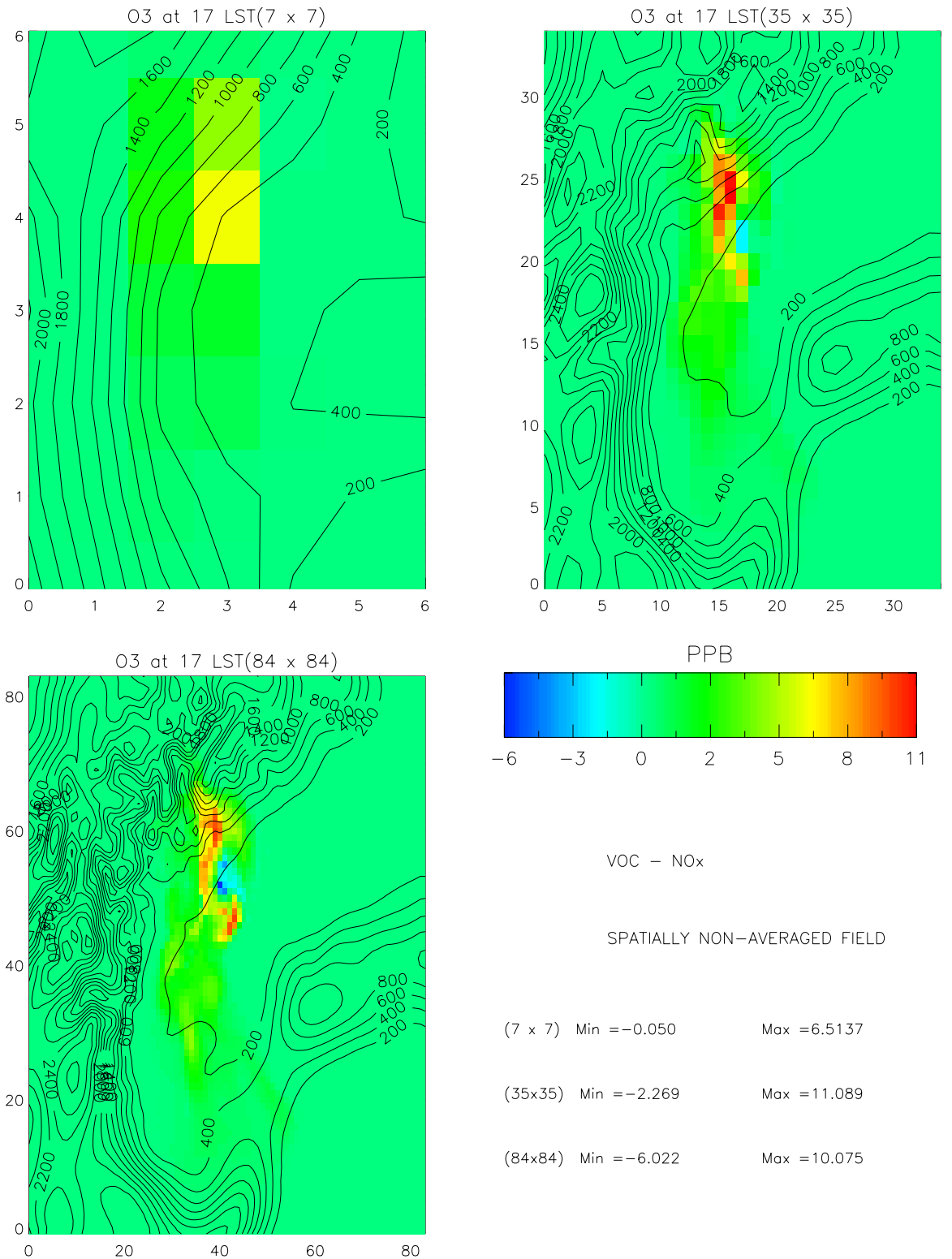


Figure 14: Comparison of chemical regimes for O3 at 17:00 LST. Chemical regime maps are obtained by subtracting the NOx emission scenario results from the VOC ones. Positive areas indicate a NOx sensitive regime whereas negative areas are representative of a VOC sensitive regime.

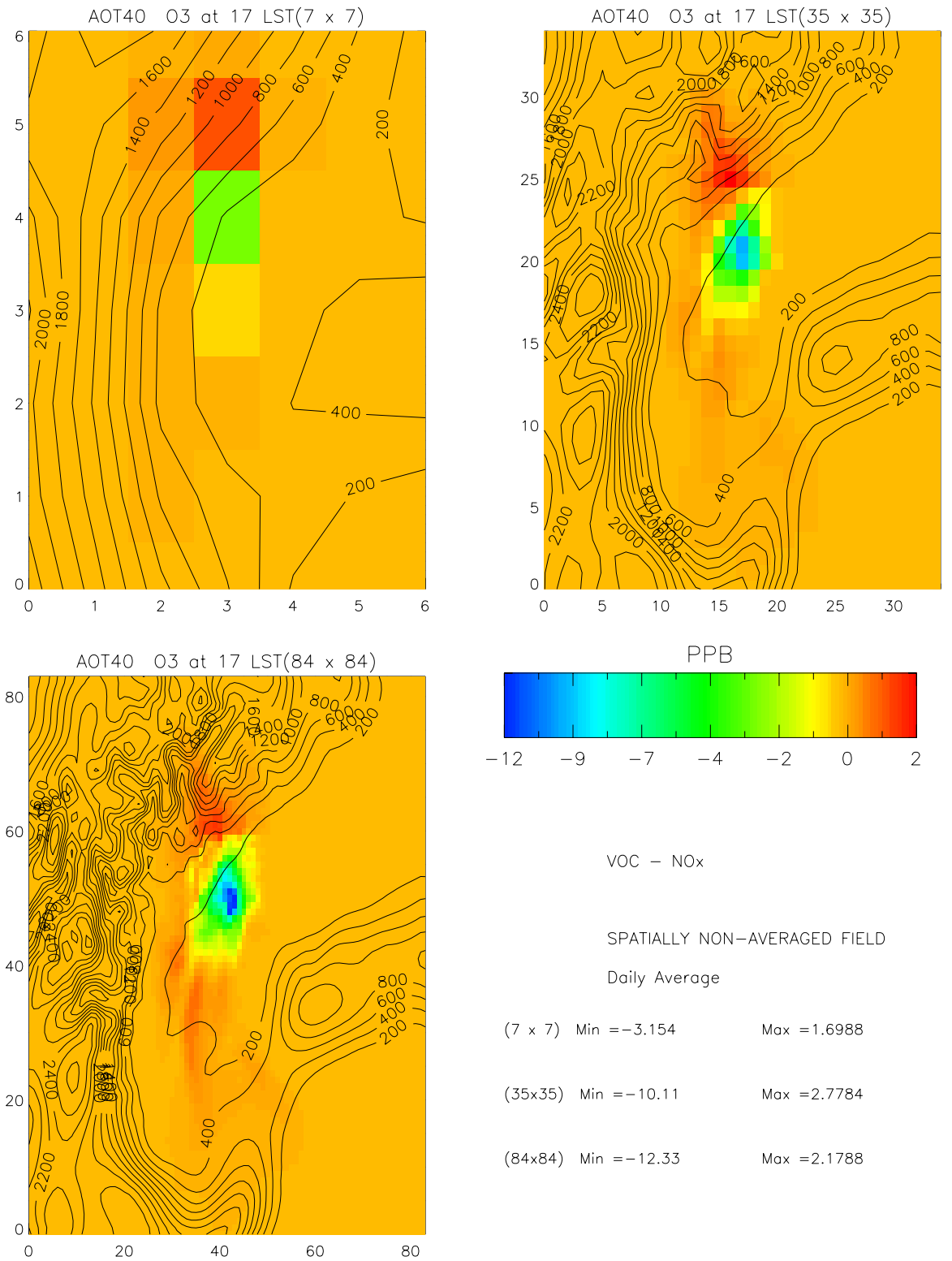


Figure 15: Same as Figure 14 but for daily AOT-40.

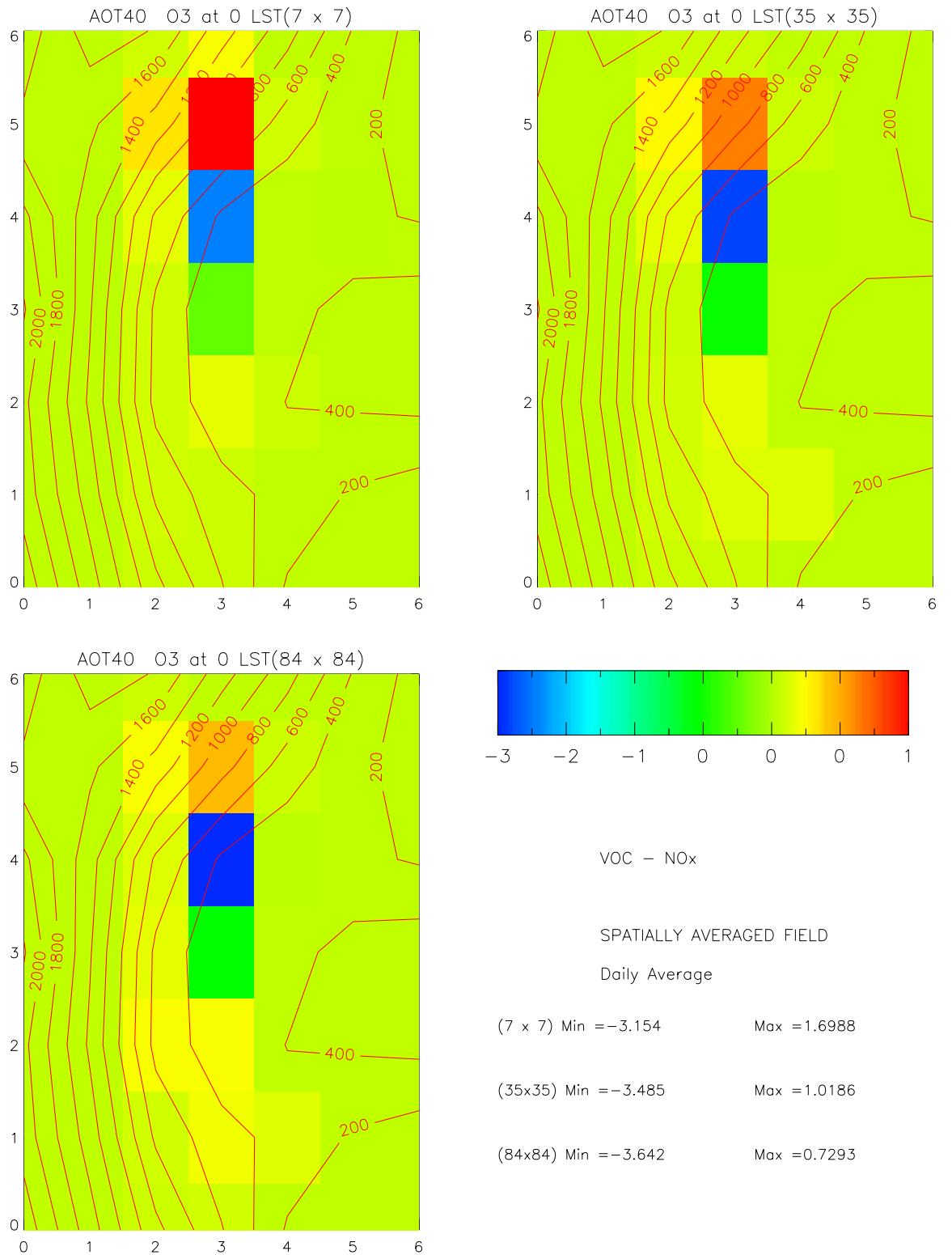


Figure 16: same as Figure 15 but for spatially averaged daily AOT-40.

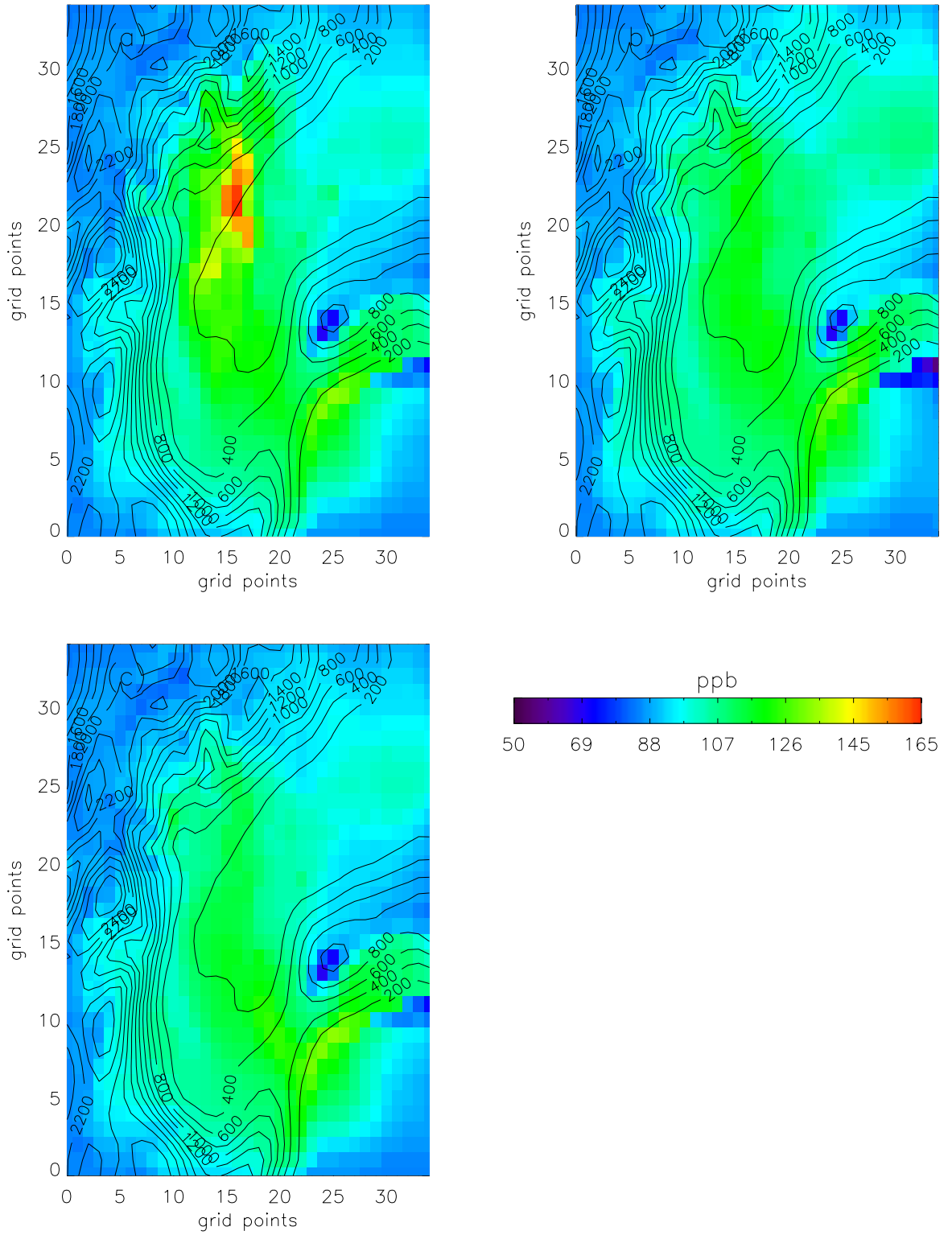


Figure 17: TAPOM results on the 10x10 grid (R5) obtained for O₃ at 17:00 LST with (a) the full emission inventory, (b) the EMEP emission inventory and (c) the EMEP emissions but assumed constant throughout the day

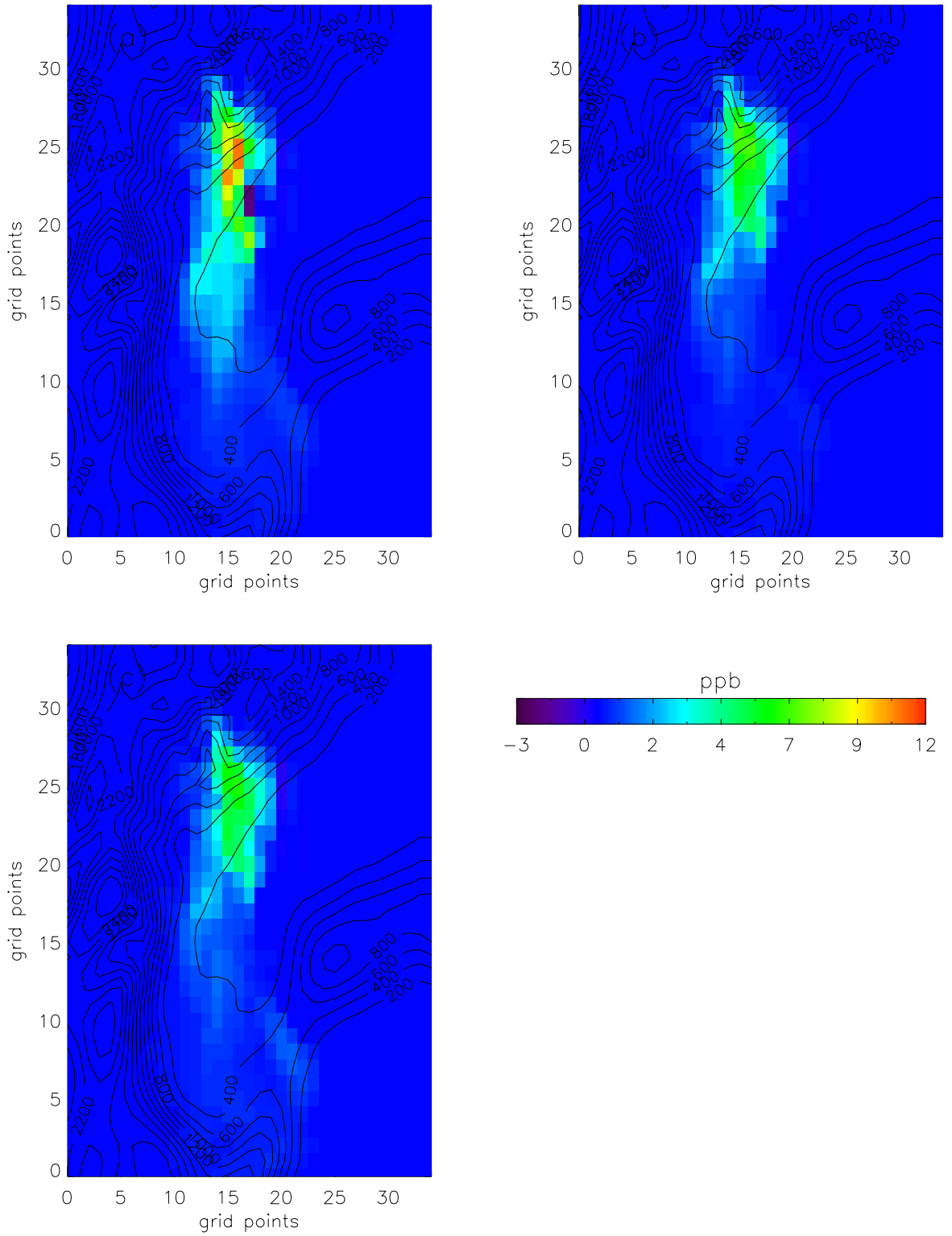


Figure 18: TAPOM results on the 10x10 grid (R5) obtained for VOC-NOx sensitivities at 17:00 LST with (a) the full emission inventory, (b) the EMEP emission inventory and (c) the EMEP emissions but assumed constant throughout the day

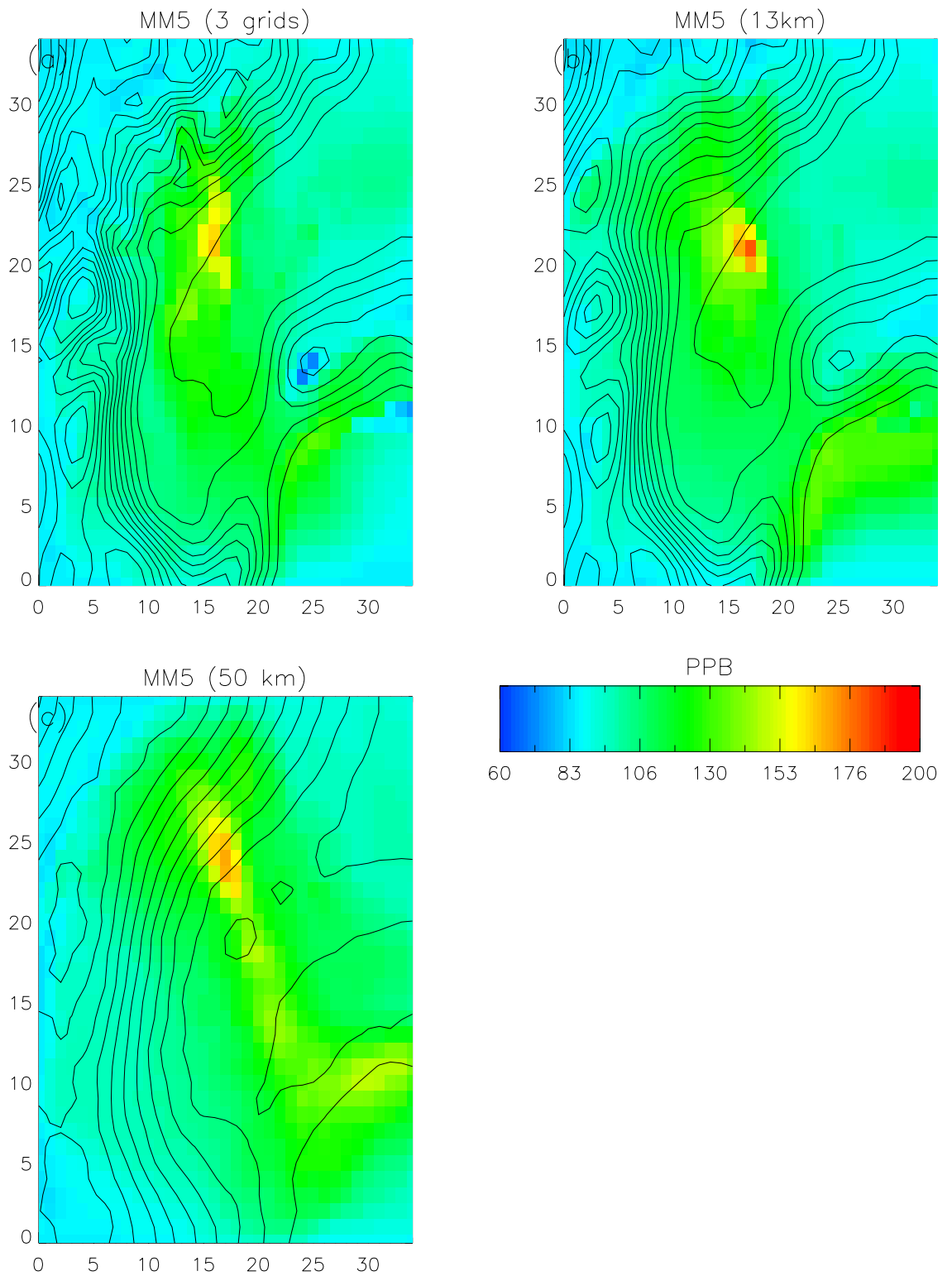


Figure 19: Comparison of O3 at 17:00 LST with R5 for three different resolution for the MM5 meteorological datasets: (a) three 2-way nested grids with resolution of 1.5, 4.5 and 13.5 km, (b) one single grid with 13.5 km resolution and (c) one single grid with 50 km resolution

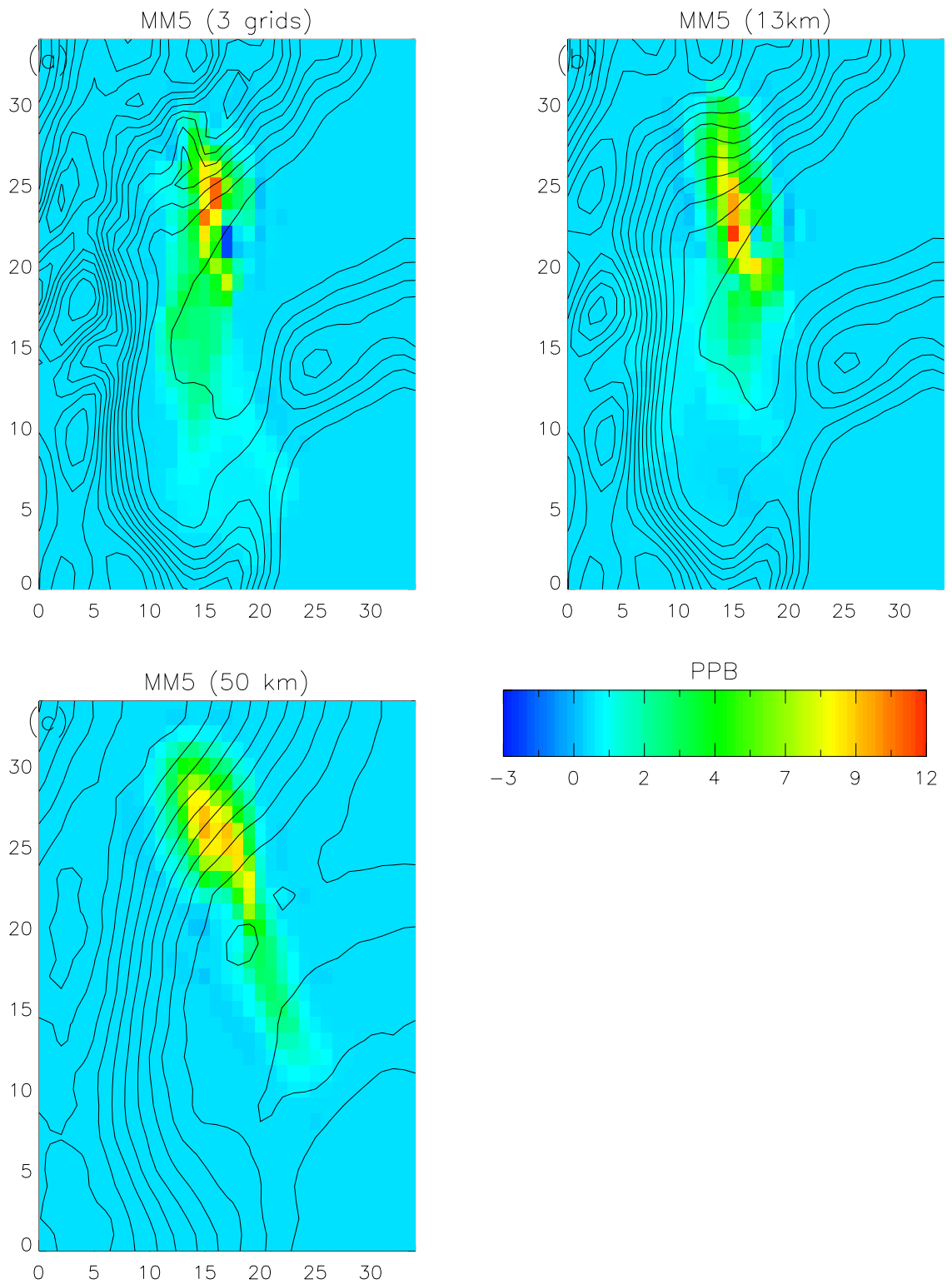


Figure 20: Comparison of VOC-NO_x sensitivities at 17:00 LST with R5 for three different resolutions for the MM5 meteorological datasets: (a) three 2-way nested grids with resolution of 1.5, 4.5 and 13.5 km, (b) one single grid with 13.5 km resolution and (c) one single grid with 50 km resolution

10. Influence of the emission inventory on air quality modelling

From the previous section, it resulted that a 10 km resolution was accurate enough to capture the relevant physical and chemical processes involved in the Milan area. Based on this, three different simulations have been performed on this 10 km grid using TAPOM. The first uses the combined emission inventory described above (Figure 17a), the second one uses the EMEP emission inventory (Figure 17b) and the third one (Figure 17c) is based on the EMEP inventory but with constant in time emissions throughout the course of the day. We clearly see that the combined emission inventory is responsible for the generation of the Milan O₃ plume. Peak values reach there 165 ppb whereas they are limited to 135 in the two other simulations. Maximum concentrations in these two latter runs are observed in Genova and not in Milan. The higher NMVOC/NO_x ratio of the fine scale emission inventory favours O₃ production in a NO_x dominated environment as Milan city is but it must be noted that both the NMVOC/NO_x ratio and the spatial resolution are different in the two inventories. Further work will thus be necessary to estimate which of these two factors is more critical in explaining the large differences (30 ppb) obtained in O₃ concentrations.

Results obtained with and without considering a time variation of the emissions are almost similar. Chemical regimes (figure 18) are geographically similarly located but the fine scale emission inventory is responsible for much stronger NO_x and VOC regimes. Being very localised in the vicinity of Milan city, the VOC sensitive regime almost disappears in the simulations carried out with the EMEP emission inventory.

11. Influence of meteorological resolution on air quality modelling

The MM5 modelling system has been used in this section in three different configurations. A first simulation is made in the configuration that has been described in the above sections, i.e. with three 2-way interactive nested grids of resolutions 1.5, 4.5 and 13.5 km. A second and third simulations are obtained by using only one single grid having a resolution of 13.5 and 50 km, respectively. Three meteorological datasets with different resolutions are then obtained. Each of these three meteorological datasets is then interpolated to the TAPOM R5 grid (i.e. 35 x 35 grid points with resolution of about 10 km) according to the procedure described in the previous sections. TAPOM simulations obtained with each of this meteorological dataset are compared. Figure 19 shows the comparison of the O₃ concentration fields obtained with the three meteorological resolutions. The location of the peak ozone concentration around Milan is similar in all three simulations although located further north in the coarser 50 km simulation. The shape of the plume is also different and tends to be more diffuse as resolution gets coarser, especially in the area of Genova. The highest concentration (181 ppb) is obtained with 13.5 single grid simulation whereas the single 50 km grid gives 169 ppb and the three nests one 164 ppb. As can be seen from those values the uncertainty on peak concentrations due to the horizontal resolution of meteorology is almost of the same order of magnitude as the uncertainty due to the variation of horizontal resolution of the photochemical model (see section 9). In the area of Genova (south east of the domain), the coarse resolution simulations tend to predict high O₃ concentrations above the sea in an area, which is largely overestimated. In fact, the lack of spatial resolution leads to associating sea type of land-use to large areas where mixing is relatively weak, generating therefore large O₃ concentrations. In this area where sharp changes of land use are present, the lack of resolution is clearly responsible for a large error in the results.

Figure 20 shows the comparison of the VOC-NO_x sensitivities for the three different meteorological resolutions. First, the VOC sensitive regime (dark blue area) is only visible in the fine resolution simulation whereas the intensity of the NO_x sensitive regime (red-green area) is slightly underestimated by the 50 km simulation while almost similar for the two finer resolution simulations. One can note that the variability of the results is relatively large in terms of location. The NO_x sensitive region not only extends further north (in agreement with the O₃ field) in the 50 km simulation than in the two others but the peak of the NO_x sensitive regime is also located differently in the three simulations. On the other hand, variations do not appear to be coherent with the increase of resolution, which points out to the non-linearity of the meteorological models. In conclusion, the variability associated to meteorological resolution is as large as the variability associated with the resolution of the air quality model. For the latter, an increase of resolution was clearly associated to a higher accuracy of the results, which is not seen for what concerns the meteorological resolution.

12. Conclusions

Spatial resolution in air pollution and meteorology modelling has always been a crucial issue. Ideally, simulations should use a resolution as fine as possible and a domain as large as possible to capture all processes. Unfortunately, this is prevented by CPU limitations. Therefore a compromise must be found between the resolution and the extent of the domain we want to simulate. The key issue consists thus in identifying the size of the relevant processes to determine the optimal scale and resolution. The goal of the present work has been to check which resolution was necessary to simulate the relevant processes in air quality modelling around cities. Simulations with different spatial resolutions were carried out and compared with a special emphasis on O₃ peaks and also on policy related indicators (AOT-40, AOT-60, ...).

A lack of spatial resolution may arise from different part of a modelling system. It includes the emission data, the meteorological data and the air pollution model itself. This work has been divided into three main sections, each one dealing with the impact of resolution on one of these air quality modules. As a test case, the PIPAPO episode on May 13th in the Po valley (Italy) has been selected. All simulations were carried out with the TAPOM air quality model.

Impact of Air Quality Model resolution

Ozone concentration fields obtained with similar meteorology and emissions but with different spatial resolutions produced similar O₃ surface field patterns. Significant differences were obtained for peak concentrations (~20%) between the 10 and 50 km resolution simulations whereas the 4 and 10 km simulation gave similar results. While peak concentrations were shown to be underestimated in coarse resolution simulations, 50 km spatially averaged concentrations were overestimated. This is explained by the larger dilution of the NO_x emissions in coarse grids that favours O₃ production. Spatially averaged errors for daily AOT-40, 8h AOT-60 and AOT-100 show an increase from 3% for the first to 15 and 20% for the second and third indicators. In summary, the 10 km resolution simulation was shown to behave very similarly to the 4 km resolution one indicating that a 10 km resolution was sufficient to reproduce accurately both O₃ peak and AOT-40 and AOT-60 values. Significant differences were only observed for AOT 100. On the other hand, the 50 km resolution produced accurate results for spatially averaged

O3 concentrations and for AOT-40 whereas errors became larger when considering AOT-60 or AOT-100.

Two emission reduction scenarios consisting in reducing by 40% first the NO_x and second the VOC emissions in the Milan city have been considered. In the NO_x scenario, variations in O₃ concentrations were similar for each spatial resolution. Spatially averaged differences were overestimated by the coarse simulations. In the VOC scenario, O₃ variations were also similar in all simulations but spatially averaged differences were in this case underestimated in the coarse resolution simulations. Coarser grids tend therefore to underestimate the impact of a VOC emission reduction and to overestimate the impact of a NO_x emission reduction. This was confirmed by the analysis of the VOC-NO_x sensitive areas which indicated an overestimation of the NO_x sensitive regime whereas the VOC sensitive regime was underestimated. This behaviour was shown to be more marked for the AOT-100 indicator than for the daily AOT-40 one.

Impact of the emission inventory

For what concerns emission, two inventories, one at 3 km and the other at 50 km have been compared and have shown to be substantially different. A factor of two difference has been identified for some compounds such as NMVOC. More important was the ratio NMVOC/NO_x shown to be larger in the 3 km inventory. As expected, these inventory differences produced significant differences in air quality outputs. Indeed, Milan plume was only reproduced by the fine scale inventory and differences as large as 30 ppb in peak values were obtained. Note that both the NMVOC/NO_x ratio and the resolution being different in these two inventories, further work will be necessary to estimate which of these two factors was more critical in explaining the large differences obtained in O₃ concentrations. The time variation of emissions during the day was shown to produce relatively low impacts.

Impact of the resolution of meteorology

Finally, the comparison of air quality results obtained with different resolution meteorological datasets has shown a similar pattern for the pollution plume although differences in resolution ranged from 1.5 to 50 km. Even a very coarse resolution of 50 km was able to capture the main features of the atmospheric circulations in the Milan region. On the other hand, the variability of O₃ levels as simulated with the different meteorological resolutions was shown to be significant and at least as important as the variability associated with the resolution of the air pollution model itself. In the area of Genova, where sharp changes in land-use are present (coastline), the impact of the spatial resolution of meteorology was shown to produce also large errors in O₃ concentrations.

Although these conclusions are in theory valid only for the specific area of Milan and only for May 13th 1998, one can expect a similar behaviour in other conditions. It will be the purpose of further work to check how valid these conclusions are on the long term as well as for other cities in Europe .

References:

Clappier et al.: Effect of sea-breeze on Air pollution in the greater Athens area. Part I: Numerical simulations and field observations. *J. Appl. Meteor.*, 39, 546-562.

Clappier, 1998: A correction method for use in multidimensional time-splitting advection algorithms: Application to two- and three dimensional transport. *Mon. Wea. Rev.*, 126, 232-242.

Collela and Woodward, 1984: The Piecewise Parabolic Method (PPM) for gas dynamical simulations. *J. Comput. Phys.*, 54, 174-201.

Grell G., J. Duddhia and D. Stauffer, 1994: A description of the fifth-generation Penn State/NCAR Mesoscale Model (MM5). NCAR/TN-398+STR

Madronich S, and S. Flocke, 1998: The role of solar radiation in atmospheric chemistry. *Handbook of Environmental chemistry* (P. Boule Ed.), Springer Verlag, Heidelberg, pp 1-26.

Middleton P., W. Stockwell, and W. Carter, 1990: Aggregation and Analysis of Volatile Organic Compound Emissions for Regional Modelling. *Atmos env*, 24, 1107-1133

Thunis P. and C. Cuvelier, 2000: Impact of biogenic emissions on ozone formation in the Mediterranean area- A BEMA modelling study. *Atmospheric Environment*, 34(3), 467-481.

Vestreng V. and E. Storen, 2000: Analysis of UNECE/EMEP Emission data MSC-W Status Report 2000. EMEP MSC-W Note 1/00.

ANNEX I: Transformation from EMEP to RACM species

As an example, let's take EMEP species NC_4H_{10} that contribute to Middleton categories 3 to 7 and 27 to 30. From the NAPAP emission data, we obtain that the sum of all emissions for those categories is equal to 8722 Gg/year. For species C_2H_5OH , the categories are only from 27 to 30 whose total mass is equal to 2075. The following relations give the mass repartition of these two species into the different categories:

$$\begin{aligned} \text{Mid_class_mass (3)} &= 124/8722 * NC_4H_{10} \\ \text{Mid_class_mass (4)} &= 1397/8722 * NC_4H_{10} \\ \text{Mid_class_mass (5)} &= 2029/8722 * NC_4H_{10} \\ \text{Mid_class_mass (6)} &= 2492/8722 * NC_4H_{10} \\ \text{Mid_class_mass (7)} &= 605/8722 * NC_4H_{10} \\ \text{Mid_class_mass (27)} &= 97/8722 * NC_4H_{10} + 97/2075 * C_2H_5OH \\ \text{Mid_class_mass (28)} &= 801/8722 * NC_4H_{10} + 801/2075 * C_2H_5OH \\ \text{Mid_class_mass (29)} &= 878/8722 * NC_4H_{10} + 878/2075 * C_2H_5OH \\ \text{Mid_class_mass (30)} &= 299/8722 * NC_4H_{10} + 299/2075 * C_2H_5OH \end{aligned}$$

To obtain the molecular repartition, we divide by each Middleton class molecular weight (see table 2) as follows:

$$\begin{aligned} \text{Mid_class_mol (3)} &= 124/8722 * NC_4H_{10}/44 \\ \text{Mid_class_mol (4)} &= 1397/8722 * NC_4H_{10}/58 \\ \text{Mid_class_mol (5)} &= 2029/8722 * NC_4H_{10}/79 \\ \text{Mid_class_mol (6)} &= 2492/8722 * NC_4H_{10}/110 \\ \text{Mid_class_mol (7)} &= 605/8722 * NC_4H_{10}/175 \\ \text{Mid_class_mol (27)} &= [97/8722 * NC_4H_{10} + 97/2075 * C_2H_5OH]/52 \\ \text{Mid_class_mol (28)} &= [801/8722 * NC_4H_{10} + 801/2075 * C_2H_5OH]/47 \\ \text{Mid_class_mol (29)} &= [878/8722 * NC_4H_{10} + 878/2075 * C_2H_5OH]/69 \\ \text{Mid_class_mol (30)} &= [299/8722 * NC_4H_{10} + 299/2075 * C_2H_5OH]/74 \end{aligned}$$

To transfer these Middleton categories into RACM species we follow the procedure proposed by Stockwell et al. (1993) with the aggregation factors (see Table 2). HC3 has for contributors classes 3, 4, 27 and 28 so that

$$\begin{aligned} \text{HC3_mass} &= [\text{Mid_class_mol}(3) * 0.57 + \text{Mid_class_mol}(4) * 1.11 + \\ &\quad \text{Mid_class_mol}(27) * 0.49 + \text{Mid_class_mol}(28) * 1.37] * \text{HC3_mw} \\ &= 0.26537 * NC_4H_{10} + 0.51448 * C_2H_5OH \\ \text{HC5_mass} &= [\text{Mid_class_mol (5)} * 0.97 + \text{Mid_class_mol (29)} * 1.07] * \text{HC5_mw} \\ &= 0.31805 * NC_4H_{10} + 0.47244 * C_2H_5OH \\ \text{HC8_mass} &= [\text{Mid_class_mol (6)} * 0.94 + \text{Mid_class_mol (7)} * 1.14 + \\ &\quad \text{Mid_class_mol (30)} * 1.15] * \text{HC8_mw} \\ &= 0.39058 * NC_4H_{10} + 0.25528 * C_2H_5OH \end{aligned}$$

The same relations hold for C_3H_6

$$\text{Mid_class_mol (10)} = 444/1537 * C_3H_6 / 42$$

$$\text{Mid_class_mol (11)} = 331/1537 * C_3H_6 / 66$$

$$\text{Mid_class_mol (12)} = 762/1537 * C_3H_6 / 68$$

$$\begin{aligned} \text{And therefore OLT_mass} &= [\text{Mid_class_mol (10)} * 1 + \text{Mid_class_mol (11)} * 1] * \text{OLT_mw} \\ &= 0.4259 * C_3H_6 \end{aligned}$$

$$\text{OLI_mass} = \text{Mid_class_mol (12)} * 1.0 = 0.4958 * C_3H_6$$

For **O-Xylene**:

$$\text{Mid_class_mol (14)} = 602/4186 * \text{Oxyl} / 78$$

$$\text{Mid_class_mol (15)} = 1556/4186 * \text{Oxyl} / 96$$

$$\text{Mid_class_mol (16)} = 2028/4186 * \text{Oxyl} / 118$$

$$\begin{aligned} \text{Which leads to: TOL_mass} &= [\text{Mid_class_mol (14)} * 0.29 + \text{Mid_class_mol (15)} * 1] * \text{TOL_mw} \\ &= 0.4054 \text{ Oxyl} \end{aligned}$$

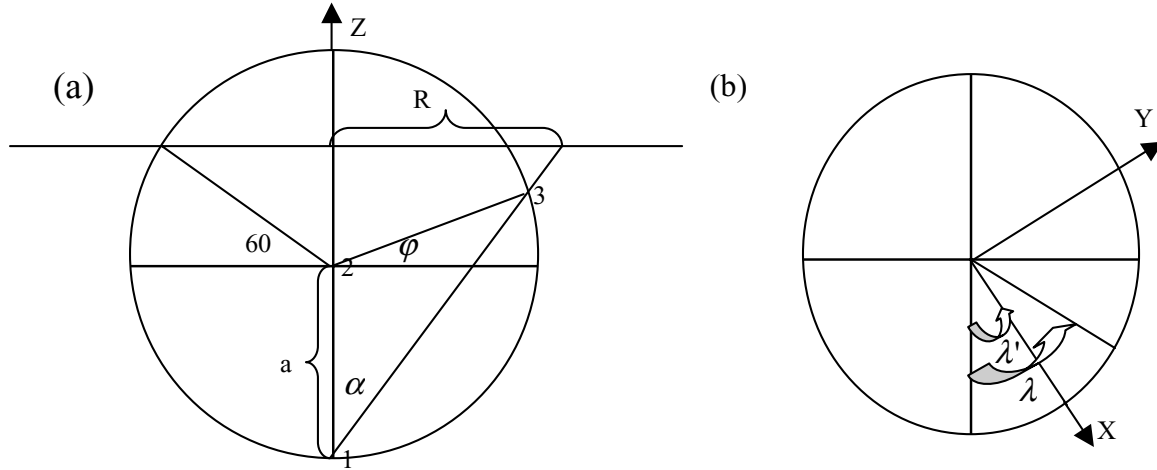
$$\text{XYL_mass} = [\text{Mid_class_mol (16)} * 1.0] * \text{XYL_mw} = 0.4352 \text{ Oxyl}$$

For $CH_3COCH_2CH_3$

$$\begin{aligned} \text{KET_mass} &= [210/397 * CH_3COCH_2CH_3 / 58 * 0.33 + 187/397 * \\ &CH_3COCH_2CH_3 / 83 * 0.61] * 72 = 0.4659 * CH_3COCH_2CH_3 \end{aligned}$$

ANNEX II: Conversion from MM5 data to the TAPOM grid

The origin of the TAPOM grid is located at the earth centre and X and Y axes are rotated according to the centre longitude of the MM5 outer domain. The following two figures illustrate the relations between MM5 and TAPOM coordinate systems.



Vertical (a) and horizontal (b) earth sections showing relations between the TAPOM and MM5 coordinate systems.

In figure (a), the triangle 1-2-3 is 'isocele so that: $\alpha + \phi + 90 + \alpha = 180 \Rightarrow \alpha = (90 - \phi) / 2$
And R is therefore given by: $R = a(1 + \sin 60) \sin \alpha$

Finally, the coordinate transformation is given by:

$$\begin{cases} x = R \cos(\lambda - \lambda') \\ y = R \sin(\lambda - \lambda') \\ z = a \sin 60 + z' \end{cases}$$

where λ, λ' , and z' are the longitude of any given point, the longitude of the MM5 outer domain centre and the height of the TAPOM levels, respectively.

Wind speeds are corrected as:

$$\begin{cases} U(\text{tapom}) = -v(\text{MM5}) \\ V(\text{tapom}) = u(\text{MM5}) \\ W(\text{tapom}) = w(\text{MM5}) \end{cases}$$

	Space Aver.	Time Aver.	R1	R5	R12	R1-R12 (%)	R5-R12 (%)			
Base Case	O3	no	no	135,5	164,4	170,1	-34,6	-20,3	-5,7	-3,4
		no	8h	124,2	141,2	146,7	-22,5	-15,3	-5,5	-3,7
		no	day	86,7	93,6	93,4	-6,7	-7,2	0,2	0,2
		yes	no	135,5	134,1	129,6	5,9	4,6	4,5	3,5
		yes	8h	124,2	118,4	114,7	9,5	8,3	3,7	3,2
		yes	day	86,7	86,5	84,9	1,8	2,1	1,6	1,9
	AOT 40	no	day	46,7	53,6	53,4	-6,7	-12,5	0,2	0,4
		yes	day	46,7	46,7	45,1	1,6	3,5	1,6	3,5
	AOT 60	no	8h	64,2	81,2	86,7	-22,5	-26,0	-5,5	-6,3
	yes	8h	64,2	58,4	54,7	9,5	17,4	3,7	6,8	
AOT100	no	no	35,5	64,4	70,1	-34,6	-49,4	-5,7	-8,1	
	yes	no	35,5	34,1	29,6	5,9	19,9	4,5	15,2	
	diff Nox									
40% NOx Reduction	O3	no	no	-10,3	-18,4	-19,7	9,4	-47,7	1,3	-6,6
		no	8h	-7,5	-10,9	-11,1	3,6	-32,4	0,2	-1,8
		no	day	-2,4	-4,6	-4,3	1,9	-44,2	-0,3	7,0
		yes	no	-10,3	-9,5	-8,5	-1,8	21,2	-1,0	11,8
		yes	8h	-7,5	-5,5	-4,4	-3,1	70,5	-1,1	25,0
		yes	day	-2,4	-1,5	-1,1	-1,3	118,2	-0,4	36,4
	AOT 40	no	day	-2,4	-4,5	-4,4	2,0	-45,5	-0,1	2,3
		yes	day	-2,4	-1,5	-1,1	-1,3	118,2	-0,4	36,4
	AOT 60	no	8h	-7,5	-10,9	-11,1	3,6	-32,4	0,2	-1,8
	yes	8h	-7,5	-5,5	-4,4	-3,1	70,5	-1,1	25,0	
AOT100	no	no	-10,3	-18,4	-19,7	9,4	-47,7	1,3	-6,6	
	yes	no	-10,3	-9,5	-8,4	-1,9	22,6	-1,1	13,1	
	diff VOC									
40% VOC Reduction		no	no	-3,8	-13,1	-16,8	13,0	-77,4	3,7	-22,0
		no	8h	-5,8	-16,7	-19,7	13,9	-70,6	3,0	-15,2
		no	day	-4,7	-9,5	-10,8	6,1	-56,5	1,3	-12,0
		yes	no	-3,8	-5,7	-5,5	1,7	-30,9	-0,2	3,6
		yes	8h	-5,8	-5,9	-5,6	-0,2	3,6	-0,3	5,4
		yes	day	-4,6	-4,4	-4,0	-0,6	15,0	-0,4	10,0
	AOT 40	no	day	-3,6	-8,1	-9,1	5,5	-60,4	1,0	-11,0
		yes	day	-3,6	-3,5	-3,2	-0,4	12,5	-0,3	9,4
	AOT 60	no	8h	-5,8	-16,7	-19,7	13,9	-70,6	3,0	-15,2
	yes	8h	-5,8	-5,9	-5,6	-0,2	3,6	-0,3	5,4	
AOT100	no	no	-3,8	-13,1	-16,8	13,0	-77,4	3,7	-22,0	
	yes	no	-4,1	-4,6	-4,3	0,2	-4,7	-0,3	7,0	

Table 1: Quantitative estimates of O3 and AOTs for different spatial and temporal averaging increments scenarios

Middleton categories (1990)	Nb	Middleton Categ. Molec. Weight	NAPAP Emission (Gg/yr)	Chemical species in RACM mechanism	RACM Species Molec. Weight	Aggreg. Factor	Chemical species in EMEP mechanism
Methane	1	16	2835	CH4	16	1	CH4
Ethane	2	30	460	ETH	30	1	C2H6
Propane	3	44	124	HC3	44	0.57	NC4H10
Alkanes							NC4H10
	4	58	1397	HC3	44	1.11	
	5	79	2029	HC5	72	0.97	
	6	110	2492	HC8	114	0.94	
	7	175	605	HC8	114	1.14	
Ethene	9	28	1267	ETE	28	1	C2H4
Propene	10	42	444	OLT	42	1	C3H6
Alkenes							C3H6
	11	66	331	OLT	42	1	
	12	68	762	OLI	68	1	
Benzene, halobenzenes	14	78	602	TOL	92	0.29	O-XILENE
Aromatics	15	96	1556	TOL	92	1	O-XILENE
Aromatics	16	118	2028	XYL	106	1	O-XILENE
Formaldehyde	19	30	320	HCHO	30	1	HCHO
Higher aldehydes	20	50	168	ALD	44	1	CH3CHO
Higher aldehydes	20	50	168	ALD	44	1	CH3CHO
Acetone, higher ketones							CH3COCH2 CH3
	21	58	210	KET	72	0.33	
	22	83	187	KET	72	0.61	
Others							C2H5OH, NC4H10
	27	52	97	HC3	44	0.49	
	28	47	801	HC3	44	1.37	
	29	69	878	HC5	72	1.07	
	30	74	299	HC8	114	1.15	

Table 2: Transformation from EMEP to RACM emission inventory